

Adverse outcomes in SARS-CoV-2 infected pregnant mice are gestational age-dependent and resolve with antiviral treatment

Patrick S. Creisher,^{1,*} Jamie L. Perry,^{1,*} Weizhi Zhong,¹ Jun Lei,^{2,3} Kathleen R Mulka,⁴ Hurley Ryan,⁵ Ruifeng Zhou,¹ Elgin H. Akin,¹ Anguo Liu,^{2,3} Wayne Mitzner,⁵ Irina Burd,^{2,3,†} Andrew Pekosz,^{1,5,†} Sabra L. Klein^{1,†}

¹W. Harry Feinstone Department of Molecular Microbiology and Immunology, The Johns Hopkins Bloomberg School of Public Health, Baltimore, Maryland, USA

²Integrated Research Center for Fetal Medicine, Department of Gynecology and Obstetrics, Johns Hopkins University School of Medicine, Baltimore, Maryland, USA

³Department of Obstetrics, Gynecology & Reproductive Sciences, University of Maryland School of Medicine, Baltimore, Maryland, USA

⁴Department of Molecular and Comparative Pathobiology, The Johns Hopkins School of Medicine, Baltimore, Maryland.

⁵Department of Environmental Health and Engineering, The Johns Hopkins Bloomberg School of Public Health, Baltimore, MD, USA.

[†]To whom correspondence should be addressed: Sabra L. Klein (sklein2@jhu.edu), Andrew Pekosz (apekosz1@jhu.edu), & Irina Burd (iburd@som.umaryland.edu)

*co-first authors

Short title: SARS-CoV-2 during mouse pregnancy

Key words: coronavirus, gestation, anti-viral, morbidity, development, Paxlovid

Manuscript statistics:

Abstract: 192 words
Text: 11812 words
Figures: 7
References: 92

28
29
30
31
32
33
34
35
36
37
38
39
40
41
42
43
44
45
46
47
48
49
50
51
52
53

Conflict of interest statement:

The authors have declared that no conflict of interest exists.
bioRxiv preprint doi: <https://doi.org/10.1101/2023.03.23.533961>; this version posted June 25, 2023. The copyright holder for this preprint (which was not certified by peer review) is the author/funder. All rights reserved. No reuse allowed without permission.

Abstract:

SARS-CoV-2 infection during pregnancy is associated with severe COVID-19 and adverse fetal outcomes, but the underlying mechanisms remain poorly understood. Moreover, clinical studies assessing therapeutics against SARS-CoV-2 in pregnancy are limited. To address these gaps, we developed a mouse model of SARS-CoV-2 infection during pregnancy. Outbred CD1 mice were infected at embryonic day (E) 6, E10, or E16 with a mouse adapted SARS-CoV-2 (maSCV2) virus. Outcomes were gestational age-dependent, with greater morbidity, reduced anti-viral immunity, greater viral titers, and more adverse fetal outcomes occurring with infection at E16 (3rd trimester-equivalent) than with infection at either E6 (1st trimester-equivalent) or E10 (2nd trimester-equivalent). To assess the efficacy of ritonavir-boosted nirmatrelvir (recommended for pregnant individuals with COVID-19), we treated E16-infected dams with mouse equivalent doses of nirmatrelvir and ritonavir. Treatment reduced pulmonary viral titers, decreased maternal morbidity, and prevented adverse offspring outcomes. Our results highlight that severe COVID-19 during pregnancy and adverse fetal outcomes are associated with heightened virus replication in maternal lungs. Ritonavir-boosted nirmatrelvir mitigated adverse maternal and fetal outcomes of SARS-CoV-2 infection. These findings prompt the need for further consideration of pregnancy in preclinical and clinical studies of therapeutics against viral infections.

54 1. Introduction:

55 Pregnancy is a risk factor for developing severe COVID-19, with pregnant individuals at

56 bioRxiv preprint doi: <https://doi.org/10.1101/2023.03.23.533961>; this version posted June 25, 2023. The copyright holder for this preprint (which was not certified by peer review) is the author/funder. All rights reserved. No reuse allowed without permission.

57 pregnant patients (1-9). The time of infection during gestation contributes to increased severity,
58 with hospitalization and intensive care unit admission being greater in the third than either the
59 second or first trimester (10, 11). While the specific mechanisms that contribute to the increased
60 risk of severe outcomes during pregnancy are not specified, both immunological and
61 physiological changes are likely involved. The immune system undergoes unique shifts as
62 pregnancy progresses, including increased regulatory T and B lymphocytes as well as reduced
63 cytotoxic and cellular immunity, to protect the developing semi-allogenic fetus (12, 13). The
64 general anti-inflammatory shift during the second and third trimesters also may increase the risk
65 of severe outcomes from viruses, including SARS-CoV-2, by blunting anti-viral immune
66 responses (13). Moreover, physiological changes associated with pregnancy including
67 cardiovascular, respiratory, endocrine, and metabolic alterations may further contribute to
68 disease severity (14). While these pregnancy-associated factors are hypothesized to contribute
69 to severe disease and death following infection with SARS-CoV-2, the exact mechanisms
70 contributing to severe COVID-19 disease during pregnancy in humans remain unknown.

71 In addition to causing severe outcomes in pregnant patients, SARS-CoV-2 infection during
72 pregnancy also can result in adverse fetal outcomes including preterm birth, stillbirth, small size
73 for gestational age, and reduced birth weight (5, 15-19), as well as increased risks of
74 neurobehavioral deficits and delayed motor skills in infants born to infected mothers (20, 21).
75 Like maternal disease, adverse perinatal and fetal outcomes appear to be influenced by
76 gestational age, with greater risk observed after infection in the third as compared with either
77 the second or first trimester (10, 20, 22). Direct placental infection or vertical transmission of
78 SARS-CoV-2 is exceedingly rare (23-25), and thus is unlikely to be the source of adverse fetal

79 and neonatal outcomes. The exact mechanisms underlying these adverse outcomes remain
80 unknown.

81 bioRxiv preprint doi: <https://doi.org/10.1101/2023.03.28.530961>; this version posted June 25, 2023. The copyright holder for this preprint (which was not certified by peer review) is the author/funder. All rights reserved. No reuse allowed without permission.

82 individuals are prioritized for receipt of available emergency use authorized antivirals and
83 vaccines (26-28), despite being excluded from clinical trials of SARS-CoV-2 vaccines and
84 antivirals (29). SARS-CoV-2 mRNA vaccines have been proven to be safe and effective during
85 pregnancy (30-32), and the United States Centers for Disease Control and Prevention
86 recommends vaccination for people who are pregnant, recently pregnant, or trying to become
87 pregnant (30). The safety and efficacy of SARS-CoV-2 antivirals during pregnancy has not been
88 as well studied. In the United States, pregnant people are recommended to receive the
89 antivirals remdesivir (brand name Veklury) and ritonavir-boosted nirmatrelvir (brand name
90 Paxlovid) when indicated (33). While neither antiviral included pregnant people in their clinical
91 trials (34), observational studies of remdesivir indicate its safety and efficacy in pregnant
92 populations (35). Nirmatrelvir is an oral antiviral that inhibits the SARS-CoV-2 M^{PRO} protease
93 and is packaged with ritonavir, a previously established HIV protease inhibitor and
94 pharmacologic booster, which does not have direct antiviral effects on SARS-CoV-2 but instead
95 works to prolong the bioavailability of nirmatrelvir through the inhibition of the hepatic
96 cytochrome P-450 (CYP) 3A4 enzyme (36, 37). Ritonavir-boosted nirmatrelvir treatment during
97 pregnancy appears safe, with no adverse obstetric outcomes reported in small observational
98 studies (38-40). The efficacy of ritonavir-boosted nirmatrelvir in preventing SARS-CoV-2
99 infection or disease during pregnancy remains an open question, in part because most studies
100 to date were not designed to evaluate efficacy (38-40).

101 Animal models of microbial infections during pregnancy provide mechanistic insight into
102 adverse maternal and fetal outcomes by enabling deeper analysis of vertical transmission and
103 maternal and fetal immune responses. Animal models have elucidated the pathogenesis of
104 infections such Zika virus, influenza A virus, *Plasmodium falciparum*, and Group B

105 *Streptococcus* infections during pregnancy (26). In the absence of human clinical trials, animal
106 models of infection during pregnancy can be used to characterize the safety and efficacy of
107 therapeutics in this high-risk population. To date, published animal models of SARS-CoV-2
108 infection during pregnancy have been limited (25, 41), which has hindered investigation into
109 both host and viral factors that may underlie the severe outcomes observed in humans. Animal
110 models have only been used to study the potential reproductive toxicity of nirmatrelvir in rats,
111 rabbits, and zebrafish, with no evidence of embryonic toxicity, fetal abnormalities, maternal
112 toxicity, or other adverse outcomes (42, 43). Whether equivalent dosing of nirmatrelvir
113 administered during pregnancy is equally efficacious against SARS-CoV-2 infection in
114 pregnancy as in nonpregnant animals has not been reported.

115 In the current study, we developed a mouse model of SARS-CoV-2 infection during
116 pregnancy to investigate maternal and offspring outcomes associated with severe COVID-19
117 disease during pregnancy and elucidate the contribution of gestational age, pulmonary and
118 placental involvement in adverse outcomes, and control of virus replication. Further, we sought
119 to assess the efficacy of ritonavir-boosted nirmatrelvir in limiting virus replication, preventing
120 maternal disease, and mitigating adverse offspring outcomes. Our results demonstrate that
121 SARS-CoV-2 infection during late gestation causes more severe maternal disease and adverse
122 offspring outcomes than infections earlier during gestation, with maternal disease and adverse
123 offspring outcomes associated with reduced pulmonary anti-viral type 1 interferon (IFN)
124 responses, greater viral replication in the lungs, and loss of placental trophoblasts. Treatment
125 with ritonavir-boosted nirmatrelvir not only reduced pulmonary virus replication, but prevented
126 severe disease and adverse fetal outcomes, highlighting additional benefits of antiviral
127 treatment during pregnancy.

128

129 **2 Materials and Methods:**

130 *2.1 Viruses and cells*

bioRxiv preprint doi: <https://doi.org/10.1101/2023.03.23.533961>; this version posted June 25, 2023. The copyright holder for this preprint (which was not certified by peer review) is the author/funder. All rights reserved. No reuse allowed without permission.

131 A mouse adapted strain of SARS-CoV-2 (maSCV2), originally generated by Dr. Ralph
132 Baric (44) was obtained from the Biodefense and Emerging Infections Research Resources
133 Repository (BEI Resources #NR-55329). The maSCV2 virus was originally generated via
134 infectious clone technology using the sequence of SARS-CoV-2/human/USA/WA-CDC-
135 02982586-001/2020 (WA1 strain) with added mutations in the Spike protein that were predicted
136 to increase binding to murine ACE2(45). This virus was further adapted to mice by sequential
137 passage to generate increased virus replication and disease(44). Working stocks of maSCV2
138 virus were generated by infecting Vero-E6-TMPRSS2 cells at a multiplicity of infection (MOI) of
139 0.01 tissue culture infectious dose 50 (TCID₅₀) per cell in infection media [Dulbecco's Modified
140 Eagle Medium (DMEM; Sigma # D5796) supplemented with 2.5% filter-sterilized fetal bovine
141 serum (Gibco# 10-437-028), 100 U/ml penicillin and 100 µg/ml streptomycin (Gibco #15149-
142 122), 1 mM l-glutamine (Gibco #2503081), and 1-mM sodium pyruvate (Gibco #11-360-070)].
143 Approximately 72 hours post infection, the supernatant fluids were collected, clarified by
144 centrifugation (400g for 10 minutes), and stored in aliquots at -70°C.

145 2.2 Experimental mice

146 Adult (8-12 weeks of age) timed pregnant and nonpregnant female CD-1 IGS mice were
147 purchased from Charles River Laboratories. Pregnant mice arrived on embryonic day (E) 4, E8,
148 and E14 and were singly housed, and nonpregnant female mice were housed at 5 per cage
149 before and after inoculation. Mice were housed under standard animal biosafety level three
150 (ABSL3) housing conditions with *ad libitum* food and water. Mice were given at least 24 hours to
151 acclimate to the ABSL3 facility prior to infections (46). All monitoring and experimental
152 procedures were performed at the same time each day.

153 2.3 SCV2 infections and monitoring

154 All animal experiments and procedures took place in an ABSL3 facility at the Johns
155 Hopkins School of Medicine. Experimental pregnant mice were intranasally infected at E6, E10,

156 or E16 with 10^5 TCID₅₀ of maSCV2(44) in 30 μ l of DMEM (Sigma #D5796) or mock inoculated
157 with 30 μ l of media. Dose-response studies in nonpregnant inbred female mice indicate that

158 maSCV2 requires doses of 10^4 or 10^5 TCID₅₀ to cause disease in adult mice (44). bioRxiv preprint doi: <https://doi.org/10.1101/2023.03.23.533961>; this version posted June 25, 2023. The copyright holder for this preprint (which was not certified by peer review) is the author/funder. All rights reserved. No reuse allowed without permission.

159 intranasal infection, mice were anesthetized via intraperitoneal ketamine/xylazine cocktail (80
160 mg/kg ketamine, 5 mg/kg xylazine). Following intranasal infections, body mass and clinical signs
161 of disease were monitored once daily in the morning for 14 days or until tissue collection.

162 Clinical scores, determined in the home cage, were administered to mice on a scale of 0-4, with
163 one point given for piloerection, dyspnea, hunched posture, and absence of an escape
164 response on each day (47, 48). Clinical scores over the course of 14 days for each animal were
165 summed to give a cumulative clinical disease score.

166 *2.4 Antiviral treatment*

167 Experimental animals were administered vehicle alone [1% (w/v) Soluplus (BASF
168 #50539897), 1% (w/v) Tween 80 (Sigma #59924), 0.5% (w/v) methylcellulose (Sigma #94378)
169 in purified water], high dose nirmatrelvir alone (300mg/kg; MedChem Express #HY-138687), or
170 an animal equivalent dose of nirmatrelvir boosted with ritonavir [1.7 mg nirmatrelvir/dose
171 (MedChem Express #HY-138687), 0.6 mg ritonavir/dose (Sigma #(#155213-67-5)]. Animal
172 equivalent doses were calculated as described (49) by converting the standard human dose of
173 nirmatrelvir and ritonavir (50) to a body-surface-area equivalent for mice (49) using a
174 standardized body surface area for mice of 0.007 mg/m². According to the United States Food
175 and Drug Administration, this calculation is recommended for conversion of animal doses to
176 human equivalent doses (51), along with an assumed mass of 30g for all calculations so that
177 pregnant and nonpregnant animals receive the same amount per dose. Mice were administered
178 treatment via oral gavage twice daily for 5 days or until tissue collection, starting 4 hours after
179 infection as described in the original published pre-clinical study of nirmatrelvir (52).

180 *2.5 Offspring measurements and behavior*

181 Offspring from mock inoculated dams and maSCV2 infected dams were measured at
182 postnatal day (PND) 0, within 12 hours of birth. Body mass (g), length measured from nose to
183 anus (mm), and head diameter measured from ear to ear (mm) were recorded for each pup,
184 directly, using a caliper, and the average for each independent litter was calculated to avoid
185 confounding litter effects. Pups at PND5 were subjected to developmental neurobehavioral
186 assays of surface righting, cliff aversion, and negative geotaxis as described (53, 54). For each
187 test, 1–2 male and 1–2 female offspring from at least 5 independent litters were used per
188 condition to avoid confounding litter effects. Pups were subjected to 3 attempts at each test,
189 with the time to complete each test recorded on a stopwatch. The upper limit of time was 60
190 seconds, 30 seconds, and 60 seconds for surface righting, cliff aversion, and negative geotaxis,
191 respectively. The pups' best trial for each test was used for analysis.

192 *2.6 Diffusion capacity of carbon monoxide*

193 To measure lung function of experimental mice, diffusion capacity for carbon monoxide
194 (DF_{CO}) was measured. Modifications to a previously published protocol (55) were made for
195 application in ABSL3. Mice were anesthetized with ketamine/xylazine cocktail (80 mg/kg
196 ketamine, 5 mg/kg xylazine). Mice were tracheostomized with an 18-G stub needle. For each
197 mouse, two 3 ml syringes containing 0.8 ml of ~0.5% neon (Ne, an insoluble inert tracer gas),
198 ~0.5% carbon monoxide (CO), and balanced air were pre-filled and sealed with a 4-way stop
199 cock. Following tracheostomy, gas was injected into the tracheostomy stub-needle to inflate the
200 lungs for two seconds and held for eight seconds. After eight seconds, the 0.8 ml volume was
201 withdrawn back into the syringe in two seconds and the syringe's stop cock closed, then the gas
202 in the syringe was diluted to 2 ml with room air and resealed. This was repeated using the
203 second syringe for each mouse. Mice were euthanized via cervical dislocation. The closed
204 syringes were decontaminated in an oven at 75°C for 15 minutes within the ABSL3 to inactivate
205 any virus in the gas sample. DF_{CO} was measured using gas chromatography as previously
206 described (55).

207 2.7 Tissue and serum collection

208 Experimental dams (infected at E6, E10, or E16) or nonpregnant female mice were

209 euthanized at 3 days post-infection. Mice were anesthetized via isoflurane and exsanguination
bioRxiv preprint doi: <https://doi.org/10.1101/2023.03.28.533961>; this version posted June 25, 2023. The copyright holder for this preprint (which was not certified by peer review) is the author/funder. All rights reserved. No reuse allowed without permission.

210 was performed via cardiac puncture. At the time of euthanasia, the total number of viable and

211 nonviable fetuses was quantified for each pregnant dam. Fetal viability was determined as the

212 percentage of fetuses within uterine horns that were viable. Fetuses were counted as nonviable

213 if they were smaller or discolored compared to gestational age-matched live fetuses or if a fetus

214 was absent at an implantation site (54, 56, 57). Maternal lungs were collected, separated by

215 lobe, and flash frozen on dry ice for homogenization. The left lung was inflated and fixed in zinc

216 buffered formalin (Thermo Fisher Scientific #NC9351419) for at least 72 hours in preparation for

217 histology. Fetuses and placenta were flash frozen in dry ice or fixed in 4% paraformaldehyde

218 (Thermo Fisher Scientific #J19943.K2) for 72 hours at 4°C for immunohistochemistry. Serum

219 was separated by blood centrifugation at 5,000 rpm for 30 min at 4°C. A subset of uninfected

220 pregnant (E16) and nonpregnant adult mice were euthanized and the median liver lobe was

221 collected and flash frozen in dry ice for Western blot.

222 2.8 Pulmonary histopathology

223 Fixed lungs were sliced into 3-mm blocks, embedded in paraffin, sectioned to 5 μ m,

224 mounted on glass slides, and stained with hematoxylin and eosin (H&E) solution to evaluate

225 lung inflammation. Semiquantitative histopathological scoring was performed by a board-

226 certified veterinary pathologist, blinded to study group assignments and outcomes, to measure

227 both severity of inflammation and the extent of inflammation (58-60). Severity of perivascular

228 and peribronchiolar mononuclear inflammation was scored on a scale of 0- to 4 (0, no

229 inflammation; 1, 1 cell layer; 2, 2-3 cell layers; 3, 4-5 cell layers; 4, > 5 cell layers). Severity of

230 alveolar inflammation was scored on a scale of 0-4 (0, no inflammation; 1- increased

231 inflammatory cells in alveoli, septa clearly distinguished; 2 – inflammatory cells fill alveoli, septa

232 clearly distinguished; 3 – inflammatory cells fill multiple adjacent alveoli, septa difficult to
233 distinguish; 4 – inflammatory cells fill multiple adjacent alveoli with septal necrosis). Extent of
234 inflammation was scored separately for perivascular, peribronchiolar, and alveolar areas on a
235 scale of 0 to 4 (0, no inflammation; 1, 2-25% tissue affected; 2, up to 50% tissue affected; 3, up
236 to 75% tissue affected; 4, >75% of tissue affected). Individual scores were summed to give a
237 cumulative inflammation score.

238 *2.9 Infectious virus and viral genome copy number quantification and tissue inactivation*

239 Frozen right cranial lungs, nasal turbinates, placentas, and fetuses were homogenized in lysing
240 matrix D bead tubes (MP Biomedicals #6913100). Homogenization media [500ml DMEM
241 (Sigma # D5796), 5ml penicillin/streptomycin (Gibco #15149-122)] was added to bead tubes
242 containing tissue at a minimum volume of 400 μ l and maximum volume of 1200 μ l (10% w/v) and
243 homogenized at 4.0m/s for 45s in a MP Fast-prep 24 5G instrument. After homogenization, the
244 supernatant was divided in half and transferred to two new microcentrifuge tubes. Triton X-100
245 was added to one of the transferred supernatants to a final concentration of 0.5% and incubated
246 at room temp for 30 minutes to inactivate maSCV2. Infectious and inactivated homogenates
247 were stored at -80°C. Infectious virus titers in tissue homogenate or sera were determined by
248 TCID₅₀ assay. Tissue homogenates or sera were serially diluted in infection media in
249 sextuplicate into 96-well plates confluent with Vero-E6-TMPRSS2 cells, incubated at 37°C for
250 six days. After incubation, 10% neutral buffered formalin was added to all wells to fix cells prior
251 to staining and left overnight. Formalin was discarded and the plates were stained with naphthol
252 blue black stain for visualization. Infectious virus titers were determined via the Reed and
253 Muench method. Viral RNA copy number was determined by quantitative polymerase chain
254 reaction (qPCR). A 200 μ L aliquot of tissue homogenate or serum was mixed with 1 mL of
255 TRIzol reagent (Invitrogen, Cat#15596026) for RNA extraction. To this, 200 μ L of chloroform
256 (Fisher Scientific, Cat#C298-500) was added, followed by centrifugation at 12,000 x g for 15

257 minutes at 4°C. The clear supernatant was collected and an equal volume of 100% isopropyl
258 alcohol (Fisher Scientific, Cat#A416) was added. This mixture was centrifuged at 12,000 x g for
259 10 minutes at 4°C. The resulting RNA pellet was washed with 75% ethanol (Fisher Scientific,
260 Cat#BP2818-500), air-dried, and resuspended in 50 µL of nuclease-free water. The RT-qPCR
261 for SARS-CoV-2 N1 gene detection was carried out by adding 2.5 µL of the isolated RNA into a
262 master mix composed of 2.5 µL TaqPath™ 1-Step Multiplex Master Mix (Applied Biosystems,
263 Cat#A28526), 0.75 µL of N1 SARS-CoV-2 RUO qPCR Primer & Probe Kit (IDT,
264 Cat#10006713), and 4.25 µL of nuclease-free water. This mix was added to each well of a
265 MicroAmp™ Optical 384-Well Reaction Plate (Applied Biosystems, Cat#4309849). Serial
266 dilutions of N1 were prepared in 10-fold increments for absolute quantification of copy number.
267 Each sample and standard were run in duplicate. The QuantStudio 12K Flex Real-Time PCR
268 System (Applied Biosystems) was used for amplification, and data analysis was performed
269 using the Design & Analysis Software 2.6.0 to identify SARS-CoV-2 N1.

270 *2.10 Placental histology and immunohistochemistry*

271 Placentas were fixed for 72 hours at 4°C in 4% PFA in the ABSL3. Placentas were
272 washed five times with PBS and immersed in 30% sucrose until saturation. Using a Leica
273 CM1950 cryostat, the specimens were cut at 20-µm thickness and mounted on positively
274 charged slides (Fisher Scientific #12-550-15). Routine H&E staining was performed to evaluate
275 the morphological change of the placentas. Within H&E-stained sections, mononucleated
276 trophoblast giant cells, distinguished by their large size and the presence of a single condensed
277 dark blue-purple stained nucleus, were identified and counted under a magnification of 20x. For
278 each placenta, six random images in the labyrinth at the middle level (thickest) of placenta were
279 taken and the count was averaged. For immunohistochemical staining, slides were washed with
280 PBS, which was followed by permeabilization in PBS solution containing 0.05% Triton X-100
281 and 10% normal goat serum (Invitrogen #50197Z) for 30 min. Placentas were incubated with
282 rabbit anti-vimentin (1:200, Abcam # ab92547), or rabbit anti-cytokeratin (1:200, Dako #Z0622)

283 overnight at 4°C. The next day, sections were rinsed with PBS and then incubated with donkey
284 anti-rabbit (ThermoFisher #R37119) fluorescent secondary antibodies (ThermoFisher #R37115)
285 diluted 1:500 for 3h at room temperature. DAPI (Roche #10256276001) was applied for
286 counterstaining, followed by mounting with Fluoromount-G (eBioscience #00-4958-02). Images
287 were taken using a Zeiss Axioplan 2 microscope (Jena, Germany) under 5x or 20x
288 magnification. Cell density of vimentin and cytokeratin positive cell quantification was performed
289 using Image J (1.47v). The 20x images were captured from the same batch of experiments,
290 utilizing identical imaging parameters, including exposure time for quantification. After setting
291 the appropriate scale and threshold for positive expression, the percentage of positive
292 expression relative to the entire area was calculated. For each placenta, six random images in
293 the labyrinth at the middle level (thickest) of placenta were taken, and the average fluorescent
294 area calculated for that placenta. One placenta per dam was used and 4–5 dams per group
295 were analyzed.

296 *2.11 Cortical thickness measurement*

297 A subset of offspring was randomly selected to be euthanized via decapitation at PND 0
298 and heads were fixed for 72 hours at 4°C in 4% PFA in the ABSL3. Fetal heads were washed
299 five times with PBS and immersed in 30% sucrose until saturation. Using a Leica CM1950
300 cryostat, the specimens were cut at 20- μ m thickness and mounted on positively charged slides
301 (Fisher Scientific #12-550-15). Nissl staining was performed, and images were taken under \times 5
302 magnification using a Canon EOS Rebel (Tokyo, Japan). Coronal cortical thickness was
303 measured from five random sections at the striatum level of each neonatal brain, as previously
304 described (57). Cortical thickness was measured from both brain hemispheres in each section
305 using ImageJ software, and the average of 10 measurements per specimen was presented.
306 Quantification shown represents the average measurement from a single randomly chosen pup
307 for each dam.(57)

308 *2.12 Interferon β and Interleukin 1 β ELISA*

309 Interferon β in inactivated right cranial lung or placental homogenate was measured by
310 ELISA according to the manufacturer's protocol (PBL Assay Science # 42410-1). Interleukin-1 β
311 in inactivated placental homogenate was measured by ELISA according to the manufacturer's
312 protocol (Abcam #100704).

313 2.13 Western Blot

314 Flash frozen median liver lobes were homogenized in 1X Cell lysis Buffer (Cell Signaling
315 Technology #9803) with 1X Protease Inhibitor cocktail (Sigma-Aldrich #P8340) and sodium
316 fluoride (Fisher Scientific #S299 100) (20 μ l lysis buffer per mg tissue). Protein lysates were
317 stored at -80°C until analysis. Protein concentration of each lysate was measured using the
318 Pierce BCA Protein Assay Kit (Thermo Fisher Scientific #23225). For each sample, 20 μ g of
319 protein was subjected to sodium dodecyl sulfate-polyacrylamide gel electrophoresis (SDS-
320 PAGE) on NuPAGE 4-12% Bis-Tris gels (Thermo Fisher Scientific #NP0329). The gel was
321 blotted onto Immobilon-FL PVDF Membrane (Millipore #IPFL00010) and the membranes were
322 blocked with a 1:1 mixture of 1XPBS/Tween-20 solution (Sigma-Aldrich #P3563) and Intercept
323 blocking buffer (LI-COR Biosciences #927-70001) for 30 minutes at room temperature.
324 Membranes were treated with a primary antibody diluted in blocking solution at 4°C overnight on
325 a rocker. Membranes were then washed with PBS-Tween three times and incubated in
326 secondary antibody solutions for one hour at room temperature on a rocker. Membranes were
327 washed three times in PBS-Tween and then imaged on a ProteinSimple FluoroChem Q imager.
328 Individual bands were quantified using Image Studio software (LI-COR Biosciences; version
329 3.1.4) The signal from each band was normalized against the GAPDH signal and graphed as
330 arbitrary units. Primary antibodies used were rabbit anti-P450 3A4/CYP3A4 (abcam #ab3572)
331 and mouse anti-GAPDH (abcam #ab82450). Secondary antibodies included goat anti- mouse
332 Alexa Fluor 488 (Thermo Fisher Scientific #A11001) and donkey anti-rabbit Alexa Fluor Plus
333 647 (Thermo Fisher Scientific #A32795).

bioRxiv preprint doi: <https://doi.org/10.1101/2023.03.23.533961>; this version posted June 25, 2023. The copyright holder for this preprint (which was not certified by peer review) is the author/funder. All rights reserved. No reuse allowed without permission.

334 2.14 Viral RNA extraction, sequencing, and analysis

335 For each sample, 200µl of right cranial lung or nasal turbinate homogenate was mixed

336 bioRxiv preprint doi: <https://doi.org/10.1101/2023.03.23.533961>; this version posted June 25, 2023. The copyright holder for this preprint
with (which was not certified by peer review) is the author/funder. All rights reserved. No reuse allowed without permission.

337 #C298-500) to extract RNA, and centrifuged at 12,000 g for 15 minutes at 4°C. The clear portion

338 of the supernatant was then pelleted at 12,000 g for 10 minutes along with 500µl of 100%

339 isopropyl alcohol (Fisher #A416) at 4°C. Pelleted RNA was then washed with 75% of ethanol

340 (Fisher Scientific #BP2818-500), air dried and resuspended in 20µl of nuclease-free

341 water. Reverse transcription was carried out using ProtoScript® II First Strand cDNA Synthesis

342 Kit (New England Biolabs #E6560S) with random hexamer mix. The Mpro region was then

343 amplified using forward primer 5' ACAAGATAGCACTTAAGGGTGG 3' and reverse primer 5'

344 GCGAGCTCTATTCTTTGCACTAA 3' and Oxford Nanopore sequenced by Plasmidsaurus

345 (SNPsaurus LLC). Consensus sequences for lung and turbinate virus isolates were imported

346 and aligned to Mpro ORF (NC_045512.2) using ClustalO v1.2.3 in Geneious Prime v2023.0.4.

347 Alignments were imported into R v4.1.1, visualized, and annotated using seqvisR v0.2.5.

348 ORF1a and nonstructural protein annotation was visualized using BioRender. Raw FASTQ files

349 for Mpro sequencing has been deposited through SRA under BioProject PRJNA940500 at

350 accession numbers SRR23689223 - SRR23689259.

351 2.15 Statistical analyses

352 Post infection body mass changes were plotted and the area under the curve (AUC) was

353 calculated to provide individual data points that captured change over time, with AUCs

354 compared with either two tailed unpaired t-test or two-way analysis of variance (ANOVA)

355 followed by *post-hoc* Bonferroni multiple comparisons tests. To compare body mass changes

356 across gestational ages, individual AUCs were subtracted from the average AUC of mock mice

357 at the same gestational age, with the difference from mock AUC compared with two-way

358 ANOVAs followed by *post-hoc* Bonferroni multiple comparisons test. Cumulative clinical scores

359 were analyzed using the Kruskal-Wallis test. Viral titers in lungs from infected dams were
360 analyzed using one-way or two-way ANOVAs followed by *post-hoc* Bonferroni multiple
361 comparisons test. Western blot quantification, IHC quantification, and cortical thickness
bioRxiv preprint doi: <https://doi.org/10.1101/2023.03.29.533961>; this version posted June 25, 2023. The copyright holder for this preprint
(which was not certified by peer review) is the author/funder. All rights reserved. No reuse allowed without permission.
362 measurements were analyzed with two-tailed unpaired t tests. Cumulative inflammation scoring,
363 DFCO, IFN- β , and fetal measurements were analyzed with two-way ANOVAs followed by *post-*
364 *hoc* Bonferroni multiple comparisons test. Pup neurodevelopment results were analyzed with
365 two-way or three-way ANOVAs followed by *post-hoc* Bonferroni multiple comparisons test. Fetal
366 viability data were analyzed with a χ^2 test. Data are presented as mean \pm SEM or as the
367 median (cumulative clinical score). Mean or median differences were considered statistically
368 significant at $p < 0.05$. Statistical analyses were performed using GraphPad Prism v9.5
369 (GraphPad Software).

370 *2.16 Data availability*

371 Raw FASTQ files for Mpro sequencing has been deposited through SRA under
372 BioProject PRJNA940500 at accession numbers SRR23689223 - SRR23689259. Other data
373 supporting the conclusions of this article are available in the supporting data values.

374 *2.17 Study approval*

375 All animal procedures were approved by the Johns Hopkins University Animal Care and Use
376 Committee (MO21H246). SARS-CoV-2 was handled in a BSL-3 containment facility using
377 institution approved biosafety protocols (P2003120104).

378 **3 Results:**

379 *3.1 Mouse adapted SARS-CoV-2 causes morbidity in pregnant mice, which increases with* 380 *gestational age*

381 To evaluate if SARS-CoV-2 caused greater disease in pregnant than nonpregnant mice
382 and if maternal morbidity was impacted by gestational age, we intranasally inoculated outbred
383 pregnant CD1 dams at E6, E10, or E16, roughly corresponding developmentally to human first,
384 second, or third trimesters, respectively (61), or age-matched nonpregnant females with

385 maSCV2(44) or media and measured body mass change as a measure of morbidity.
 386 Nonpregnant females (**Figure 1A**) and dams infected at E6 (**Figure 1B**) experienced mild
 387 morbidity, losing significant body mass (i.e. approximately 10% of their initial body mass by 4
 388 days post infection (dpi)), but then appearing indistinguishable from mock-inoculated females by
 389 7 dpi. In contrast, dams infected at E10 (**Figure 1C**) or E16 (**Figure 1D**) experienced prolonged
 390 maternal morbidity, with E10-infected dams gaining less body mass for the remainder of
 391 gestation than mock inoculated dams (**Figure 1C**), and E16-infected dams failing to regain body
 392 mass for the remainder of gestation or during lactation as compared to mock-inoculated dams
 393 (**Figure 1D**). No mortality was observed in any group. To compare the impact of gestation on
 394 maternal morbidity, the change in body mass relative to gestational-age matched mock-
 395 inoculated animals (**Figure 1E**) and cumulative clinical scores of disease (**Figure 1F**) were
 396 analyzed. maSCV2 infection of pregnant dams at E16 resulted in greater body mass loss and
 397 clinical disease than infection of either nonpregnant females or dams at either E6 or E10.
 398 Pregnancy and gestational age increase the severity of SARS-CoV-2 outcomes in mice,
 399 consistent with human COVID-19 data (1, 10).

400 *3.2 Pregnant dams infected late in gestation have reduced IFN- β responses, increased viral* 401 *load, and reduced pulmonary function after infection*

402 Deficits in type 1 IFN signaling are associated with severe COVID-19 in nonpregnant
 403 people (62) and mice (63). Pregnancy is associated with downregulation of prototypical
 404 cytolytic and anti-viral pathways, including type I IFNs, and upregulation of anti-inflammatory
 405 pathways toward mid to late gestation (64). We hypothesized that E16-infected dams would
 406 have a reduced type I IFN response after SARS-CoV-2 infection compared to E6-, and E10-
 407 infected dams and nonpregnant females. To test this, we infected pregnant dams at E6, E10,
 408 and E16 as well as age-matched nonpregnant females with maSCV2 or media and collected
 409 lungs at 3 dpi. Infected nonpregnant females as well as E6- and E10-infected dams had
 410 significantly increased concentrations of pulmonary IFN- β as compared with matched mock-

411 inoculated females (**Figure 2A**). In contrast, maSCV2 infection at E16 resulted in pulmonary
412 concentrations of IFN- β that were indistinguishable from vehicle-inoculated dams and

413 bioRxiv preprint doi: <https://doi.org/10.1101/2023.03.23.533964>; this version posted June 25, 2023. The copyright holder for this preprint
413 (which was not certified by peer review) is the author/funder. All rights reserved. No reuse allowed without permission.

414 maSCV2 (**Figure 2A**). To determine if reduced anti-viral IFN- β concentrations were associated
415 with greater pulmonary virus replication, at 3 dpi, we evaluated infectious viral titers (**Figure 2B**)
416 and viral N1 gene copy numbers (**Supplemental Table 1**) in the lungs of nonpregnant, E6, E10,
417 and E16 pregnant females that were maSCV2-infected. E16-infected dams had significantly
418 greater pulmonary titers of infectious virus and viral RNA than either E6-infected dams, E10-
419 infected dams, or infected nonpregnant females (**Figure 2B, Supplemental Table 1**).

420 To determine if greater viral replication contributed to worse pulmonary outcomes, at
421 3dpi, we evaluated pulmonary histopathology (**Figure 2C-D, Supplemental Figure 1**), and
422 diffusion capacity (DF_{CO}; **Figure 2E**) in the lungs of nonpregnant, E6, or E16 pregnant females
423 that were either maSCV2 or mock-infected. maSCV2 infection induced pulmonary
424 histopathological changes, including intra-alveolar necrosis and inflammatory cell debris, and
425 peribronchiolar, and perivascular mononuclear inflammatory infiltrates that were observed in
426 nonpregnant (**Supplementary Figure 1A**, representative image), E6- (**Supplemental Figure**
427 **1B**, representative image), and E16- (**Figure 2C**, representative image) infected mice (**Figure**
428 **2D**, scoring) to equivalent levels. maSCV2 infection at E16 significantly reduced pulmonary
429 function, as measured by DF_{CO}, which was not observed following maSCV2 infection at E6 or in
430 nonpregnant females. These data suggest that late gestation is associated with reduced
431 antiviral responses, greater virus replication, and reduced pulmonary function.

432 *3.3 SARS-CoV-2 infection late in gestation disrupts trophoblasts and cytokine concentrations in*
433 *the placenta*

434 As placental pathology has been observed during COVID-19 (65-67), we next
435 investigated if maSCV2 could infect or cause damage to the placenta. Dams were mock- or
436 maSCV2-infected at E10 [when the placenta is formed (61)] or E16 and euthanized at 3 dpi.

437 Placentas, fetal tissues, and maternal sera were analyzed for infectious virus and viral RNA
438 (**Supplemental Table 1**), with placentas further analyzed for tissue damage (**Figure 3**). All
439 placentas, fetal tissues, and maternal sera were negative for viral RNA and infectious virus
bioRxiv preprint doi: <https://doi.org/10.1101/2023.03.23.533961>; this version posted June 25, 2023. The copyright holder for this preprint
(which was not certified by peer review) is the author/funder. All rights reserved. No reuse allowed without permission.
440 (**Supplemental Table 1**), consistent with human reports that direct placental infection and
441 vertical transmission during COVID-19 is rare (23, 24). Despite no detectable infectious virus or
442 viral RNA, placentas from E16-infected dams had reduced numbers of mononuclear trophoblast
443 giant cells (**Figure 3A** for representative images, and **Figure 3B** for quantification), suggestive
444 of damage to the trophoblast-endothelial cell barrier, which separates maternal and fetal blood
445 in the labyrinth of the murine placenta (68). Staining for cytokeratin (trophoblasts, **Figure 3C, E**)
446 and **Supplemental Figure 2A**) and vimentin (endothelial cells, **Figure 3D, F** and **Supplemental**
447 **Figure 2B**) was performed and revealed a significant loss of trophoblasts, but not endothelial
448 cells, in placentas from E16-infected compared with mock-infected dams (**Figure 3C-F-C**).
449 These data illustrate disruption of the maternal and fetal barrier in the absence of direct viral
450 infection or vertical transmission. Moreover, cell numbers in placentas of E10-infected dams did
451 not differ from placentas of mock-inoculated dams (**Supplemental Figure 2A-B**). These data
452 suggest that placental damage may be associated with the more severe maternal disease seen
453 with infection at E16, potentially due to maternal immune activation or sickness behavior (69-
454 71), which will require further studies for elucidation.

455 Altered concentrations of cytokines, including IFN- β and IL-1 β , in the placenta are
456 associated with placental damage (56, 69, 72, 73). As such, we measured IFN β and IL-1 β in
457 placentas of dams that were maSCV2 infected or mock inoculated at E10 (**Supplemental**
458 **Figure 2C-D**) or E16 (**Figure 3G-H**). Maternal maSCV2 infection at E16, but not E10, resulted
459 in increased concentrations of IFN- β and reduced concentrations of IL-1 β in the placenta
460 relative to mock-inoculated dams (**Figure 3G-H, Supplemental Figure 2C-D**) These data
461 suggest that maSCV2 infection shifted the balance of these two counter regulatory cytokines in

462 the placenta (74, 75), with placental IFN- β and IL-1 β concentrations being correlated,
463 regardless of infection status or timing of infection (**Supplemental Figure 2E**).

464 bioRxiv preprint doi: <https://doi.org/10.1101/2023.03.23.533961>; this version posted June 25, 2023. The copyright holder for this preprint (which was not certified by peer review) is the author/funder. All rights reserved. No reuse allowed without permission.

465 **3.4 SARS-CoV-2 infection late in gestation causes intrauterine growth restriction**
466 COVID-19 during human pregnancy is associated with adverse pregnancy and fetal
467 outcomes including preterm birth, stillbirth, small size for gestational age, and reduced birth
468 weight (15). To evaluate if the maSCV2-induced maternal morbidity and placental damage
469 observed after infection at E16 was associated with adverse pregnancy or fetal outcomes, we
470 inoculated dams with maSCV2 or media at E6, E10, or E16, with a subset of dams euthanized
471 at 3 dpi to evaluate fetal viability and the remainder followed to evaluate birth outcomes. Neither
472 fetal viability (**Figure 4A**) nor litter size (**Figure 4B**) was affected by maSCV2 infection during
473 pregnancy at any gestational age. maSCV2 infection at E6 or E10 did not result in reductions in
474 fetal growth relative to fetuses from mock-inoculated dams (**Figure 4C-E**). In contrast, maSCV2
475 infection at E16 led to significantly smaller pups in terms of mass, length, and head size relative
476 to fetuses from mock-infected dams (**Figure 4C-E**). Collectively, fetuses from E16-infected
477 dams had greater growth restriction than fetuses from either E6- or E10-infected dams (**Figure**
478 **4C-E**). Reduced birth size was not mediated by pre-term birth as all dams, regardless of
479 infection, delivered at approximately E20 (76). These data indicate that maSCV2 infection
480 during the third trimester-equivalent of pregnancy results in intrauterine growth restriction, which
481 was not observed when infection occurs earlier during gestation.

481 **3.5 Offspring of SARS-CoV-2 infection late in gestation display cortical thinning and reduced**
482 *neurodevelopmental behaviors*

483 In addition to adverse perinatal outcomes, COVID-19 during pregnancy also has been
484 associated with an increased risk of neurodevelopmental disorders in infants within their first
485 year of life (20, 21). As such, we evaluated offspring of mock-inoculated or maSCV2-infected
486 dams at E16 for reduced cortical thickness at postnatal day (PND) 0 and delayed
487 neurobehavioral function at PND 5. Offspring of E16-infected dams had significant cortical

488 thinning in comparison to offspring from mock-inoculated dams (**Figure 5A-B**), consistent with
 489 their reduced head diameter (**Figure 4E**). Offspring of E16-infected dams displayed delayed
 490 surface righting (**Figure 4C**), cliff aversion (**Figure 4D**), and negative geotaxis (**Figure 4E**) as
 491 compared with offspring from mock-infected dams. Male offspring were more affected by
 492 maternal infection at E16 than female offspring, consistent with literature indicating that males
 493 are more severely impacted by *in utero* insults (77, 78), including SARS-CoV-2 infection (21).
 494 Offspring of dams that were either maSCV2- or mock-infected at E6 or E10 also were subjected
 495 to neurobehavioral testing, and no effect of either maternal infection or sex of offspring was
 496 observed (**Supplemental Figure 3**). These data highlight that infection with maSCV2 during the
 497 third trimester-equivalent of pregnancy causes both short and long-term adverse fetal
 498 outcomes, in the absence of vertical transmission and consistent with human literature (2, 20,
 499 21).

500 *3.6 Ritonavir-boosted nirmatrelvir treatment prevents morbidity and reduces pulmonary viral* 501 *titers following SARS-CoV-2 infection late in gestation*

502 Because of the increased risk of severe COVID-19 and adverse fetal outcomes,
 503 pregnant individuals are recommended to receive the antiviral ritonavir-boosted nirmatrelvir in
 504 the United States (33, 34). There is, however, limited data on its efficacy during pregnancy, with
 505 human and animal studies primarily focused on evaluating safety and toxicity (38, 42).
 506 Additionally, studies evaluating nirmatrelvir's efficacy in nonpregnant animals utilized high doses
 507 of nirmatrelvir alone in lieu of boosting with ritonavir (52, 79). To better reflect the doses
 508 administered to pregnant individuals, we first evaluated the efficacy of nirmatrelvir and ritonavir
 509 at doses calculated to be the mouse equivalent to a human doses (49) in nonpregnant females
 510 compared to high dose nirmatrelvir alone. Mouse equivalent dosing of nirmatrelvir and ritonavir
 511 was equivalent to high dose nirmatrelvir alone at preventing maSCV2 induced morbidity
 512 (**Supplemental Figure 4A**) and reducing pulmonary viral loads (**Supplemental Figure 4B**) in
 513 nonpregnant females. As CYP3A enzymes are responsible for the metabolism of nirmatrelvir

514 (80), we evaluated liver CYP3A in pregnant dams at E16 and age-matched non-pregnant
515 females and found no difference in total expression (**Figure 6A**), further supporting the use of
516 mouse-equivalent doses of nirmatrelvir and ritonavir during pregnancy.

bioRxiv preprint doi: <https://doi.org/10.1101/2023.03.23.533961>; this version posted June 25, 2023. The copyright holder for this preprint (which was not certified by peer review) is the author/funder. All rights reserved. No reuse allowed without permission.

517 To evaluate the efficacy of ritonavir-boosted nirmatrelvir during pregnancy, we treated
518 maSCV2 and mock-infected dams twice daily with mouse-equivalent doses of nirmatrelvir and
519 ritonavir or vehicle for 5 days (50), starting at 4 hours after infection. maSCV2-infected dams
520 treated with vehicle failed to gain mass during the remainder of pregnancy and had reduced
521 mass compared to mock-inoculated dams through lactation (**Figure 6B**). In contrast, treatment
522 of maSCV2-infected dams with ritonavir-boosted nirmatrelvir prevented maternal morbidity and
523 resulted in morbidity curve AUCs that were equivalent to those of mock-inoculated dams
524 (**Figure 6B**). Ritonavir-boosted nirmatrelvir did not significantly reduce infectious viral loads in
525 the nasal turbinates of pregnant or nonpregnant females (**Figure 6C**). In the lungs, however,
526 ritonavir-boosted nirmatrelvir reduced viral loads in pregnant, but not nonpregnant, females
527 compared to vehicle-treated comparators, likely because infected vehicle-treated nonpregnant
528 females already had lower viral loads than infected pregnant vehicle-treated dams (**Figure 6D**).
529 We next determined if treatment with ritonavir-boosted nirmatrelvir selected for mutations in the
530 coding region corresponding to the gene that encodes for the SARS-CoV-2 MPRO protease.
531 The sequences encoding M^{PRO} did not differ between viral RNA obtained from ritonavir-boosted
532 nirmatrelvir treated mice and vehicle treated mice, regardless of either pregnancy status or
533 tissue type (**Figure 6E, Supplemental Figure 5**), suggesting that ritonavir-boosted nirmatrelvir
534 is not selecting for mutations that would potentially reduce its efficacy, at least by 3 dpi.

535 *3.7 Ritonavir-boosted nirmatrelvir treatment prevents adverse offspring outcomes induced by* 536 *SARS-CoV-2 infection late in gestation*

537 To evaluate if ritonavir-boosted nirmatrelvir prevented adverse fetal and offspring
538 outcomes, offspring of E16-infected and mock-inoculated dams treated with ritonavir-boosted
539 nirmatrelvir, or vehicle were evaluated at birth and PND5. Offspring of maSCV2-infected dams

540 treated with vehicle were significantly smaller than offspring of mock-inoculated dams in mass
 541 (**Figure 7A**), length (**Figure 7B**), and head diameter (**Figure 7C**) at birth and demonstrated
 542 **significant delays in surface righting (Figure 7D), swim aversion (Figure 7E), and negative**
 543 **geotaxis (Figure 7F)** at PND5, with greater neurobehavioral delays in males than females
 544 (**Figure 7D-F**). Offspring of maSCV2-infected dams treated with ritonavir-boosted nirmatrelvir,
 545 however, did not differ from offspring of mock-inoculated dams in any size measures at birth
 546 (**Figure 7A-C**) or neurobehaviors at PND5 (**Figure 7D-F**). Ritonavir-boosted nirmatrelvir
 547 treatment prevented maSCV2-induced intrauterine growth restriction and neurobehavioral
 548 deficits in both males and females. Offspring of mock-inoculated dams treated with ritonavir-
 549 boosted nirmatrelvir did not differ from offspring of mock-inoculated dams in any offspring
 550 measure (**Figure 7A-F**), consistent with reproductive studies in rabbits which did not find toxicity
 551 during pregnancy (42) Overall, these findings suggest that treatment with ritonavir-boosted
 552 nirmatrelvir during pregnancy can not only reduce maternal pulmonary viral load, but prevents
 553 maternal morbidity, and mitigates adverse fetal and offspring outcomes.

554

555 **4 Discussion:**

556 Animal models of COVID-19 are powerful tools to study pathogenesis, consider risk-
 557 altering conditions such as pregnancy, and evaluate therapeutic interventions (81, 82). In the
 558 current study, we established a mouse model of SARS-CoV-2 infection during pregnancy that
 559 recapitulates many of the clinical findings of COVID-19 during human pregnancy. Pregnant
 560 dams infected with maSCV2 in late gestation experienced the most severe disease, exhibiting
 561 reduced pulmonary function and increased viral titers, while their offspring were small for
 562 gestational age and had neurodevelopmental delays. These findings are consistent with
 563 observations in humans where pregnant individuals with COVID-19, especially in mid to late
 564 gestation, have greater risk of severe disease, resulting in increased hospitalization and critical
 565 care admission (10, 11). Virological, biological, and social factors, including SARS-CoV-2

566 infectious dose and variant, preexisting immunity, and access to healthcare likely contribute to
567 the diversity of adverse fetal outcomes observed with human COVID-19 during pregnancy (15,

568 bioRxiv preprint doi: <https://doi.org/10.1101/2023.03.23.533961>; this version posted June 25, 2023. The copyright holder for this preprint (which was not certified by peer review) is the author/funder. All rights reserved. No reuse allowed without permission.

569 selective manifestation of adverse fetal outcomes, such as reduced birth mass and
570 neurodevelopmental outcomes, that are worse in male than female offspring (16, 17, 20, 21)
571 Our model did not capture other aspects of COVID-19 during pregnancy, including preterm birth
572 or stillbirth (5, 15, 18, 22), that have been observed in human cases.

573 At the maternal-fetal interface, intranasal maSCV2 infection resulted in placental
574 alterations without direct virus infection, which is in accordance with the hallmarks of placental
575 damage, inflammation, and maternal immune cell infiltration observed in placentas from
576 mothers with COVID-19 during pregnancy (65-67). After characterizing the negative outcomes
577 of maSCV2 infection in pregnancy, we used our model to assess the efficacy of ritonavir-
578 boosted nirmatrelvir at a mouse-equivalent dose to what pregnant humans receive. This
579 antiviral regimen was well tolerated by pregnant dams, reduced pulmonary virus titers, mitigated
580 maternal morbidity, and prevented adverse offspring outcomes. Observational studies in human
581 pregnancies indicate that ritonavir boosted-nirmatrelvir does not pose safety or toxicity risk to
582 pregnant individuals (38), and may reduce COVID-19 symptoms without requiring additional
583 medical interventions (39).

584 In addition to recapitulating aspects of human COVID-19 during pregnancy, our model
585 identified reduction in pulmonary IFN- β secretion after infection late in gestation and a
586 corresponding increase in pulmonary viral titer as critical mediators of worse outcomes in late
587 compared with early gestation. As deficits in type 1 IFN signaling have been associated with
588 severe COVID-19 in both nonpregnant individuals (62) and mice (63), our data suggest that
589 maternal morbidity may, in part, be due to an inability of pregnant dams to control viral
590 replication because of a reduced type I IFN responses, particularly during late gestation. This
591 potential mechanism of severe disease is consistent with immunological alterations of mouse

592 and human pregnancy where the maternal immune response shifts to an anti-inflammatory
593 profile to support the semi-allogenic fetus and diverts from anti-viral and cytotoxic activity (12).

594 bioRxiv preprint doi: <https://doi.org/10.1101/2023.03.23.533961>; this version posted June 25, 2023. The copyright holder for this preprint
(which was not certified by peer review) is the author/funder. All rights reserved. No reuse allowed without permission.
594 Moreover, in human pregnancy, there is a documented decline in early antiviral effector cells
595 and products including natural killer cells and type I IFNs (64).

596 The adverse maternal and fetal outcomes of SARS-CoV-2 infection during pregnancy
597 are like those observed in other mouse models of viral pathogenesis during pregnancy including
598 Zika virus (ZIKV) and influenza A virus (IAV) infection. Mouse models of ZIKV infection during
599 pregnancy have shown that adverse fetal and neonatal outcomes including congenital
600 abnormalities, reduced cortical thickness, and neurobehavioral deficits (54, 57), are mediated in
601 part by transplacental virus transmission and acute placental inflammation (54, 56). While
602 vertical transmission during ZIKV infection contributes to adverse outcomes, we and others
603 have shown that the maternal immune response, including elevated production of IL-1 β , also
604 plays a key role in pathogenesis (54, 84). Vertical transmission of virus during COVID-19 is
605 largely unseen in humans (23, 24, 66), and in mice the placental pathology following maSCV2
606 infection occurred without vertical transmission. These data further highlight that adverse
607 neonatal outcomes are not exclusive to vertical transmission of viruses, but by maternal immune
608 activation and damage at the maternal-fetal interface. Mouse models of IAV infection during
609 pregnancy further demonstrate maternal morbidity and mortality which is more severe in
610 pregnant than nonpregnant animals (68, 71). Reduced type I IFN responses and greater viral
611 loads in the lungs in pregnant dams late in gestation also have been observed in IAV infection
612 (85), further supporting that pregnancy-associated suppression of type I IFNs is a mechanism of
613 severe maternal disease after respiratory virus infection.

614 Mouse models of viral infection during pregnancy are a valuable tool to assess the
615 safety and efficacy of therapeutics to prevent adverse maternal and fetal outcomes. Our results
616 support the efficacy of ritonavir-boosted nirmatrelvir for COVID-19 during pregnancy. While
617 human studies of ritonavir-boosted nirmatrelvir during pregnancy are still needed, these findings

618 provide a foundation for future human clinical trial design to include pregnant patients. Current
619 approaches to assessing antiviral therapeutics in preclinical animal models include reproductive
620 bioRxiv preprint doi: <https://doi.org/10.1101/2023.03.23.533961>; this version posted June 25, 2023. The copyright holder for this preprint
toxicity studies using supraphysiological doses but neglect to evaluate if pregnancy alters
(which was not certified by peer review) is the author/funder. All rights reserved. No reuse allowed without permission.
621 efficacy (42, 86, 87). Therefore, future preclinical models of antiviral therapies must be designed
622 carefully to consider the complex interactions between pregnancy, viral pathogenesis, and drug
623 pharmacokinetics. Mouse models of ZIKV antiviral treatment during pregnancy have illustrated
624 the ability of maternal antiviral treatment to prevent vertical transmission to fetuses (88), a major
625 adverse outcome associated with ZIKV infection during pregnancy. Pregnant individuals are
626 largely excluded from clinical trials (29), which has contributed to a reduced uptake of antivirals
627 and vaccines in pregnant populations, including COVID-19 therapeutics (89, 90). This exclusion
628 is concerning because pregnant individuals and their neonates are highly vulnerable to many
629 pathogens (91, 92). With further development of mouse models of viral infection and novel
630 therapeutics in pregnancy, however, preclinical studies can guide clinical trial design and
631 promote the inclusion of pregnant populations. By considering pregnancy in clinical trials,
632 access and uptake of protective therapeutics during pregnancy can be improved.

633

634 **5 Acknowledgements:**

635 The authors would like to thank Dr. Ralph Baric as well as the Klein, Pekosz, Davis, and
636 Baumgarth laboratories for discussions about these data, and Ariana Campbell for early
637 assistance with animal studies. We would also like to thank Dr. Jason Villano and the expert
638 animal care staff at the Johns Hopkins School of Medicine for assistance with maintenance of
639 SARS-CoV-2-infected dams.

640 **6 Funding:**

641 Funding provided by NIH/NICHD R01HD097608 (I.B. and S.L.K), NIH/NIAID training grant
642 T32AI007417-26 (P.C.), and NIAID N7593021C00045 (A.P.).

643 **7 Contributions:**

644 SK, AP, IB, PC, and JP conceptualized and designed the experiments. PC and JP performed
 645 animal experiments. AP, WZ, and RZ grew and quantified viruses and homogenized and
 646 inactivated tissue. PC and JP performed ELISA and Western blot. RM imaged and scored lung
 647 histology slides. PC, JP, HR, and WM performed DFco analysis. JL and AL stained, imaged,
 648 and analyzed placental and fetal head tissue. EA analyzed sequencing data. PC and JP
 649 statistically analyzed and graphed data. PC, JP, and SK wrote the manuscript with input from all
 650 authors. All authors read and provided edits to drafts and approved the final submission. The
 651 order of authors was determined based on contributions to the overall design, experimentation,
 652 analyses, and writing.

653 **8 References:**

- 654 1. Lokken EM, Huebner EM, Taylor GG, Hendrickson S, Vanderhoeven J, Kachikis A, et al.
 655 Disease severity, pregnancy outcomes, and maternal deaths among pregnant patients
 656 with severe acute respiratory syndrome coronavirus 2 infection in Washington State.
 657 *Am J Obstet Gynecol.* 2021;225(1):77 e1- e14.
- 658 2. Woodworth KR, Olsen EO, Neelam V, Lewis EL, Galang RR, Oduyebo T, et al. Birth and
 659 Infant Outcomes Following Laboratory-Confirmed SARS-CoV-2 Infection in Pregnancy -
 660 SET-NET, 16 Jurisdictions, March 29-October 14, 2020. *MMWR Morb Mortal Wkly Rep.*
 661 2020;69(44):1635-40.
- 662 3. Laura ASC, Raghda EE, Jaiprasath S, Anna Y, Amary F, Morris CP, et al. Reduced control
 663 of SARS-CoV-2 infection is associated with lower mucosal antibody responses in
 664 pregnant women. *medRxiv.* 2023:2023.03.19.23287456.
- 665 4. Zambrano LD, Ellington S, Strid P, Galang RR, Oduyebo T, Tong VT, et al. Update:
 666 Characteristics of Symptomatic Women of Reproductive Age with Laboratory-Confirmed
 667 SARS-CoV-2 Infection by Pregnancy Status - United States, January 22-October 3, 2020.
 668 *MMWR Morb Mortal Wkly Rep.* 2020;69(44):1641-7.
- 669 5. Allotey J, Stallings E, Bonet M, Yap M, Chatterjee S, Kew T, et al. Clinical manifestations,
 670 risk factors, and maternal and perinatal outcomes of coronavirus disease 2019 in
 671 pregnancy: living systematic review and meta-analysis. *BMJ.* 2020;370:m3320.
- 672 6. Metz TD, Clifton RG, Hughes BL, Sandoval G, Saade GR, Grobman WA, et al. Disease
 673 Severity and Perinatal Outcomes of Pregnant Patients With Coronavirus Disease 2019
 674 (COVID-19). *Obstet Gynecol.* 2021;137(4):571-80.
- 675 7. Mullins E, Hudak ML, Banerjee J, Getzlaff T, Townson J, Barnette K, et al. Pregnancy and
 676 neonatal outcomes of COVID-19: coreporting of common outcomes from PAN-COVID
 677 and AAP-SONPM registries. *Ultrasound Obstet Gynecol.* 2021;57(4):573-81.

- 678 8. Jering KS, Claggett BL, Cunningham JW, Rosenthal N, Vardeny O, Greene MF, et al.
679 Clinical Characteristics and Outcomes of Hospitalized Women Giving Birth With and
680 Without COVID-19. *JAMA Intern Med.* 2021;181(5):714-7.
- 681 9. Chinn H, Sedighim S, Kirby KA, Hohnmann S, Hameed AB, Jelley J, et al. Characteristics and
682 Outcomes of Women With COVID-19 Giving Birth at US Academic Centers During the
683 COVID-19 Pandemic. *JAMA Netw Open.* 2021;4(8):e2120456.
- 684 10. Stock SJ, Carruthers J, Calvert C, Denny C, Donaghy J, Goulding A, et al. SARS-CoV-2
685 infection and COVID-19 vaccination rates in pregnant women in Scotland. *Nat Med.*
686 2022;28(3):504-12.
- 687 11. Badr DA, Picone O, Bevilacqua E, Carlin A, Meli F, Sibiude J, et al. Severe Acute
688 Respiratory Syndrome Coronavirus 2 and Pregnancy Outcomes According to Gestational
689 Age at Time of Infection. *Emerg Infect Dis.* 2021;27(10):2535-43.
- 690 12. Mor G, Cardenas I, Abrahams V, and Guller S. Inflammation and pregnancy: the role of
691 the immune system at the implantation site. *Ann N Y Acad Sci.* 2011;1221:80-7.
- 692 13. Abu-Raya B, Michalski C, Sadarangani M, and Lavoie PM. Maternal Immunological
693 Adaptation During Normal Pregnancy. *Front Immunol.* 2020;11:575197.
- 694 14. Yu W, Hu X, and Cao B. Viral Infections During Pregnancy: The Big Challenge Threatening
695 Maternal and Fetal Health. *Matern Fetal Med.* 2022;4(1):72-86.
- 696 15. Piekos SN, Price ND, Hood L, and Hadlock JJ. The impact of maternal SARS-CoV-2
697 infection and COVID-19 vaccination on maternal-fetal outcomes. *Reprod Toxicol.*
698 2022;114:33-43.
- 699 16. Smith ER, Oakley E, Grandner GW, Ferguson K, Farooq F, Afshar Y, et al. Adverse
700 maternal, fetal, and newborn outcomes among pregnant women with SARS-CoV-2
701 infection: an individual participant data meta-analysis. *BMJ Glob Health.* 2023;8(1).
- 702 17. Wei SQ, Bilodeau-Bertrand M, Liu S, and Auger N. The impact of COVID-19 on pregnancy
703 outcomes: a systematic review and meta-analysis. *CMAJ.* 2021;193(16):E540-E8.
- 704 18. DeSisto CL, Wallace B, Simeone RM, Polen K, Ko JY, Meaney-Delman D, et al. Risk for
705 Stillbirth Among Women With and Without COVID-19 at Delivery Hospitalization -
706 United States, March 2020-September 2021. *MMWR Morb Mortal Wkly Rep.*
707 2021;70(47):1640-5.
- 708 19. Fallach N, Segal Y, Agassy J, Perez G, Peretz A, Chodick G, et al. Pregnancy outcomes
709 after SARS-CoV-2 infection by trimester: A large, population-based cohort study. *PLoS*
710 *One.* 2022;17(7):e0270893.
- 711 20. Edlow AG, Castro VM, Shook LL, Kaimal AJ, and Perlis RH. Neurodevelopmental
712 Outcomes at 1 Year in Infants of Mothers Who Tested Positive for SARS-CoV-2 During
713 Pregnancy. *JAMA Netw Open.* 2022;5(6):e2215787.
- 714 21. Edlow AG, Castro VM, Shook LL, Haneuse S, Kaimal AJ, and Perlis RH. Sex-Specific
715 Neurodevelopmental Outcomes Among Offspring of Mothers With SARS-CoV-2 Infection
716 During Pregnancy. *JAMA Netw Open.* 2023;6(3):e234415.
- 717 22. Piekos SN, Roper RT, Hwang YM, Sorensen T, Price ND, Hood L, et al. The effect of
718 maternal SARS-CoV-2 infection timing on birth outcomes: a retrospective multicentre
719 cohort study. *Lancet Digit Health.* 2022;4(2):e95-e104.

bioRxiv preprint doi: <https://doi.org/10.1101/2023.05.25.533969>; this version posted June 20, 2023. The copyright holder for this preprint (which was not certified by peer review) is the author/funder. All rights reserved. No reuse allowed without permission.

- 720 23. Simbar M, Nazarpour S, and Sheidaei A. Evaluation of pregnancy outcomes in mothers
 721 with COVID-19 infection: a systematic review and meta-analysis. *J Obstet Gynaecol.*
 722 2023;43(1):2162867.
- 723 24. Vigil-Vazquez S, Carrasco-Garcia J, Hernandez-Lobo A, Manzanares A, Berez-Perez A
 724 (which was not certified by peer review) is the author/funder. All rights reserved. No reuse allowed without permission.
 725 Toledano-Revilla J, et al. Impact of Gestational COVID-19 on Neonatal Outcomes: Is
 726 Vertical Infection Possible? *Pediatr Infect Dis J.* 2022;41(6):466-72.
- 727 25. Kim B, Park KH, Lee OH, Lee G, Kim H, Lee S, et al. Effect of severe acute respiratory
 728 syndrome coronavirus 2 infection during pregnancy in K18-hACE2 transgenic mice. *Anim*
 729 *Biosci.* 2023;36(1):43-52.
- 730 26. Vermillion MS, and Klein SL. Pregnancy and infection: using disease pathogenesis to
 731 inform vaccine strategy. *NPJ Vaccines.* 2018;3:6.
- 732 27. Emanoil AR, Stochino Loi E, Feki A, and Ben Ali N. Focusing Treatment on Pregnant
 733 Women With COVID Disease. *Front Glob Womens Health.* 2021;2:590945.
- 734 28. Siberry GK, Mofenson LM, Calmy A, Reddy UM, and Abrams EJ. Use of Ritonavir-Boosted
 735 Nirmatrelvir in Pregnancy. *Clin Infect Dis.* 2022;75(12):2279-81.
- 736 29. Klein SL, Creisher PS, and Burd I. COVID-19 vaccine testing in pregnant females is
 737 necessary. *J Clin Invest.* 2021;131(5).
- 738 30. LipKind HS V-BG, DeSilva M, et al. . Receipt of COVID-19 Vaccine During Pregnancy and
 739 Preterm of Small-for-Gestational-Age at Birth- Eight Integrated Health Care
 740 Organizations, United States, December 15, 2020-July 22, 2021. *MMWR Morb Mortal*
 741 *Wkly Rep.* 2022;71:26-30.
- 742 31. Watanabe A, Yasuhara J, Iwagami M, Miyamoto Y, Yamada Y, Suzuki Y, et al. Peripartum
 743 Outcomes Associated With COVID-19 Vaccination During Pregnancy: A Systematic
 744 Review and Meta-analysis. *JAMA Pediatr.* 2022;176(11):1098-106.
- 745 32. Villar J, Soto Conti CP, Gunier RB, Ariff S, Craik R, Cavoretto PI, et al. Pregnancy
 746 outcomes and vaccine effectiveness during the period of omicron as the variant of
 747 concern, INTERCOVID-2022: a multinational, observational study. *Lancet.*
 748 2023;401(10375):447-57.
- 749 33. NIH. COVID-19 Treatment Guidelines.
 750 <https://www.covid19treatmentguidelines.nih.gov/therapies/antiviral-therapy/ritonavir-boosted-nirmatrelvir--paxlovid/>. Accessed July 14th 2022.
- 751 34. Arco-Torres A, Cortes-Martin J, Tovar-Galvez MI, Montiel-Troya M, Riquelme-Gallego B,
 752 and Rodriguez-Blanche R. Pharmacological Treatments against COVID-19 in Pregnant
 753 Women. *J Clin Med.* 2021;10(21).
- 754 35. Burwick RM, Yawetz S, Stephenson KE, Collier AY, Sen P, Blackburn BG, et al.
 755 Compassionate Use of Remdesivir in Pregnant Women With Severe Coronavirus Disease
 756 2019. *Clin Infect Dis.* 2021;73(11):e3996-e4004.
- 757 36. Hsu A, Granneman GR, and Bertz RJ. Ritonavir. Clinical pharmacokinetics and
 758 interactions with other anti-HIV agents. *Clin Pharmacokinet.* 1998;35(4):275-91.
- 759 37. Society for Maternal Fetal Medicine. FDA Issues EUA for the Treatment of Mild-to-
 760 Moderate COVID-19
 761 Maternal-Fetal Medicine Subspecialists Support Use in Pregnant Patients.
 762 https://s3.amazonaws.com/cdn.smfm.org/media/3287/Treatment_1.10.pdf. Accessed
 763 July 14th 2022.

- 764 38. William M. Garneau MD MPH KJ-BD, MSN CNM,2 Michelle O. Ufua BS,2 Heba H.
 765 Mostafa MBBCh PhD,3 Sabra L. Klein PhD,4, 5 Irina Burd MD PhD, *2 Kelly A. Gebo MD
 766 MPH*. Clinical outcomes of pregnant patients treated with Nirmatrelvir/Ritonavir for
 767 acute COVID-19: a case series of twenty-five patients from the Johns Hopkins CROWN
 768 registry. *JAMA Open*. 2022;in press.
- bioRxiv preprint doi: <https://doi.org/10.1101/2023.05.29.533061>; this version posted June 23, 2023. The copyright holder for this preprint
 (which was not certified by peer review) is the author/funder. All rights reserved. No reuse allowed without permission.
- 769 39. Loza A, Farias R, Gavin N, Wagner R, Hammer E, and Shields A. Short-term Pregnancy
 770 Outcomes After Nirmatrelvir-Ritonavir Treatment for Mild-to-Moderate Coronavirus
 771 Disease 2019 (COVID-19). *Obstet Gynecol*. 2022;140(3):447-9.
- 772 40. Lin CY, Cassidy AG, Li L, Prah MK, Golan Y, and Gaw SL. Nirmatrelvir-Ritonavir (Paxlovid)
 773 for Mild Coronavirus Disease 2019 (COVID-19) in Pregnancy and Lactation. *Obstet*
 774 *Gynecol*. 2023;141(5):957-60.
- 775 41. Lin K, Liu M, Bao L, Lv Q, Zhu H, Li D, et al. Safety and protective capability of an
 776 inactivated SARS-CoV-2 vaccine on pregnancy, lactation and the growth of offspring in
 777 hACE2 mice. *Vaccine*. 2022;40(32):4609-16.
- 778 42. Catlin NR, Bowman CJ, Champion SN, Cheung JR, Nowland WS, Sathish JG, et al.
 779 Reproductive and developmental safety of nirmatrelvir (PF-07321332), an oral SARS-
 780 CoV-2 M(pro) inhibitor in animal models. *Reprod Toxicol*. 2022;108:56-61.
- 781 43. Zizioli D, Ferretti S, Mignani L, Castelli F, Tiecco G, Zanella I, et al. Developmental safety
 782 of nirmatrelvir in zebrafish (*Danio rerio*) embryos. *Birth Defects Res*. 2023;115(4):430-
 783 40.
- 784 44. Leist SR, Dinnon KH, 3rd, Schafer A, Tse LV, Okuda K, Hou YJ, et al. A Mouse-Adapted
 785 SARS-CoV-2 Induces Acute Lung Injury and Mortality in Standard Laboratory Mice. *Cell*.
 786 2020;183(4):1070-85 e12.
- 787 45. Dinnon KH, 3rd, Leist SR, Schafer A, Edwards CE, Martinez DR, Montgomery SA, et al. A
 788 mouse-adapted model of SARS-CoV-2 to test COVID-19 countermeasures. *Nature*.
 789 2020;586(7830):560-6.
- 790 46. Creisher PS, Campbell AD, Perry JL, Roznik K, Burd I, and Klein SL. Influenza subtype-
 791 specific maternal antibodies protect offspring against infection but inhibit vaccine-
 792 induced immunity and protection in mice. *Vaccine*. 2022;40(47):6818-29.
- 793 47. Vom Steeg LG, Dhakal S, Woldetsadik YA, Park HS, Mulka KR, Reilly EC, et al. Androgen
 794 receptor signaling in the lungs mitigates inflammation and improves the outcome of
 795 influenza in mice. *PLoS Pathog*. 2020;16(7):e1008506.
- 796 48. Vom Steeg LG, Vermillion MS, Hall OJ, Alam O, McFarland R, Chen H, et al. Age and
 797 testosterone mediate influenza pathogenesis in male mice. *Am J Physiol Lung Cell Mol*
 798 *Physiol*. 2016;311(6):L1234-L44.
- 799 49. Nair AB, and Jacob S. A simple practice guide for dose conversion between animals and
 800 human. *J Basic Clin Pharm*. 2016;7(2):27-31.
- 801 50. FDA. Fact sheet for healthcare providers: emergency use authorization for paxlovid.
 802 <https://www.fda.gov/media/155050/download>. Updated 12/2021.
- 803 51. FDA. Estimating the Maximum Safe Starting Dose in Initial Clinical Trials for Therapeutics
 804 in Adult Healthy Volunteers. [https://www.fda.gov/regulatory-information/search-fda-
 805 guidance-documents/estimating-maximum-safe-starting-dose-initial-clinical-trials-
 806 therapeutics-adult-healthy-volunteers](https://www.fda.gov/regulatory-information/search-fda-guidance-documents/estimating-maximum-safe-starting-dose-initial-clinical-trials-therapeutics-adult-healthy-volunteers).

- 807 52. Owen DR, Allerton CMN, Anderson AS, Aschenbrenner L, Avery M, Berritt S, et al. An
 808 oral SARS-CoV-2 M(pro) inhibitor clinical candidate for the treatment of COVID-19.
 809 *Science*. 2021;374(6575):1586-93.
- 810 53. Feather Schussler DN, and Ferguson TS. A Battery of Motor Tests in a Neonatal Mouse
 811 Model of Cerebral Palsy. *J Vis Exp*. 2016(117):
 812 54. Lei J, Vermillion MS, Jia B, Xie H, Xie L, McLane MW, et al. IL-1 receptor antagonist
 813 therapy mitigates placental dysfunction and perinatal injury following Zika virus
 814 infection. *JCI Insight*. 2019;4(7).
- 815 55. Limjunyawong N, Fallica J, Ramakrishnan A, Datta K, Gabrielson M, Horton M, et al.
 816 Phenotyping mouse pulmonary function in vivo with the lung diffusing capacity. *J Vis*
 817 *Exp*. 2015(95):e52216.
- 818 56. Creisher PS, Lei J, Sherer ML, Dziedzic A, Jedlicka AE, Narasimhan H, et al.
 819 Downregulation of transcriptional activity, increased inflammation, and damage in the
 820 placenta following in utero Zika virus infection is associated with adverse pregnancy
 821 outcomes. *Front Virol*. 2022;2.
- 822 57. Vermillion MS, Lei J, Shabi Y, Baxter VK, Crilly NP, McLane M, et al. Intrauterine Zika
 823 virus infection of pregnant immunocompetent mice models transplacental transmission
 824 and adverse perinatal outcomes. *Nat Commun*. 2017;8:14575.
- 825 58. Meyerholz DK, and Beck AP. Histopathologic Evaluation and Scoring of Viral Lung
 826 Infection. *Methods Mol Biol*. 2020;2099:205-20.
- 827 59. Meyerholz DK, Sieren JC, Beck AP, and Flaherty HA. Approaches to Evaluate Lung
 828 Inflammation in Translational Research. *Vet Pathol*. 2018;55(1):42-52.
- 829 60. Armando F, Beythien G, Kaiser FK, Allnoch L, Heydemann L, Rosiak M, et al. SARS-CoV-2
 830 Omicron variant causes mild pathology in the upper and lower respiratory tract of
 831 hamsters. *Nat Commun*. 2022;13(1):3519.
- 832 61. Sones JL, and Davisson RL. Preeclampsia, of mice and women. *Physiol Genomics*.
 833 2016;48(8):565-72.
- 834 62. Hadjadj J, Yatim N, Barnabei L, Corneau A, Boussier J, Smith N, et al. Impaired type I
 835 interferon activity and inflammatory responses in severe COVID-19 patients. *Science*.
 836 2020;369(6504):718-24.
- 837 63. Ogger PP, Garcia Martin M, Michalaki C, Zhou J, Brown JC, Du Y, et al. Type I interferon
 838 receptor signalling deficiency results in dysregulated innate immune responses to SARS-
 839 CoV-2 in mice. *Eur J Immunol*. 2022;52(11):1768-75.
- 840 64. Alberca RW, Pereira NZ, Oliveira L, Gozzi-Silva SC, and Sato MN. Pregnancy, Viral
 841 Infection, and COVID-19. *Front Immunol*. 2020;11:1672.
- 842 65. Rad HS, Rohl J, Stylianou N, Allenby MC, Bazaz SR, Warkiani ME, et al. The Effects of
 843 COVID-19 on the Placenta During Pregnancy. *Front Immunol*. 2021;12:743022.
- 844 66. Argueta LB, Lacko LA, Bram Y, Tada T, Carrau L, Rendeiro AF, et al. Inflammatory
 845 responses in the placenta upon SARS-CoV-2 infection late in pregnancy. *iScience*.
 846 2022;25(5):104223.
- 847 67. Huynh A, Sehn JK, Goldfarb IT, Watkins J, Torous V, Heerema-McKenney A, et al. SARS-
 848 CoV-2 Placentitis and Intraparenchymal Thrombohematomas Among COVID-19
 849 Infections in Pregnancy. *JAMA Netw Open*. 2022;5(3):e225345.

- 850 68. Kim HM, Kang YM, Song BM, Kim HS, and Seo SH. The 2009 pandemic H1N1 influenza
851 virus is more pathogenic in pregnant mice than seasonal H1N1 influenza virus. *Viral*
852 *Immunol.* 2012;25(5):402-10.
- 853 69. Chudnovets A, Lei J, Na Q, Dong J, Narasimhan H, Klein SL, et al. Dose-dependent
854 structural and immunological changes in the placenta and fetal brain in response to
855 systemic inflammation during pregnancy. *Am J Reprod Immunol.* 2020;84(1):e13248.
- 856 70. Carpentier PA, Haditsch U, Braun AE, Cantu AV, Moon HM, Price RO, et al. Stereotypical
857 alterations in cortical patterning are associated with maternal illness-induced placental
858 dysfunction. *J Neurosci.* 2013;33(43):16874-88.
- 859 71. Littauer EQ, Esser ES, Antao OQ, Vassilieva EV, Compans RW, and Skountzou I. H1N1
860 influenza virus infection results in adverse pregnancy outcomes by disrupting tissue-
861 specific hormonal regulation. *PLoS Pathog.* 2017;13(11):e1006757.
- 862 72. Yockey LJ, Jurado KA, Arora N, Millet A, Rakib T, Milano KM, et al. Type I interferons
863 instigate fetal demise after Zika virus infection. *Sci Immunol.* 2018;3(19).
- 864 73. Yockey LJ, and Iwasaki A. Interferons and Proinflammatory Cytokines in Pregnancy and
865 Fetal Development. *Immunity.* 2018;49(3):397-412.
- 866 74. Mayer-Barber KD, and Yan B. Clash of the Cytokine Titans: counter-regulation of
867 interleukin-1 and type I interferon-mediated inflammatory responses. *Cell Mol Immunol.*
868 2017;14(1):22-35.
- 869 75. Guarda G, Braun M, Staehli F, Tardivel A, Mattmann C, Forster I, et al. Type I interferon
870 inhibits interleukin-1 production and inflammasome activation. *Immunity.*
871 2011;34(2):213-23.
- 872 76. Elovitz MA, Wang Z, Chien EK, Rychlik DF, and Phillippe M. A new model for
873 inflammation-induced preterm birth: the role of platelet-activating factor and Toll-like
874 receptor-4. *Am J Pathol.* 2003;163(5):2103-11.
- 875 77. Hunter SK, Hoffman MC, D'Alessandro A, Noonan K, Wyrwa A, Freedman R, et al. Male
876 fetus susceptibility to maternal inflammation: C-reactive protein and brain
877 development. *Psychol Med.* 2021;51(3):450-9.
- 878 78. Sutherland S, and Brunwasser SM. Sex Differences in Vulnerability to Prenatal Stress: a
879 Review of the Recent Literature. *Curr Psychiatry Rep.* 2018;20(11):102.
- 880 79. Uraki R, Kiso M, Iida S, Imai M, Takashita E, Kuroda M, et al. Characterization and
881 antiviral susceptibility of SARS-CoV-2 Omicron BA.2. *Nature.* 2022;607(7917):119-27.
- 882 80. Costantine MM. Physiologic and pharmacokinetic changes in pregnancy. *Front*
883 *Pharmacol.* 2014;5:65.
- 884 81. Munoz-Fontela C, Widerspick L, Albrecht RA, Beer M, Carroll MW, de Wit E, et al.
885 Advances and gaps in SARS-CoV-2 infection models. *PLoS Pathog.* 2022;18(1):e1010161.
- 886 82. Chu H, Chan JF, and Yuen KY. Animal models in SARS-CoV-2 research. *Nat Methods.*
887 2022;19(4):392-4.
- 888 83. Whipps MDM, Phipps JE, and Simmons LA. Perinatal health care access, childbirth
889 concerns, and birthing decision-making among pregnant people in California during
890 COVID-19. *BMC Pregnancy Childbirth.* 2021;21(1):477.
- 891 84. Casazza RL, Philip DT, and Lazear HM. Interferon Lambda Signals in Maternal Tissues to
892 Exert Protective and Pathogenic Effects in a Gestational Stage-Dependent Manner.
893 *mBio.* 2022;13(3):e0385721.

bioRxiv preprint doi: <https://doi.org/10.1101/2023.05.23.543394>; this version posted June 25, 2023. The copyright holder for this preprint (which was not certified by peer review) is the author/funder. All rights reserved. No reuse allowed without permission.

- 894 85. Engels G, Hierweger AM, Hoffmann J, Thieme R, Thiele S, Bertram S, et al. Pregnancy-
 895 Related Immune Adaptation Promotes the Emergence of Highly Virulent H1N1 Influenza
 896 Virus Strains in Allogeneically Pregnant Mice. *Cell Host Microbe*. 2017;21(3):321-33.
 897 86. Kala S, Watson B, Zhang JG, Papp S, Guzman-Lenis M, Deaneby M, et al. Improving the
 898 clinical relevance of a mouse pregnancy model of antiretroviral toxicity; a
 899 pharmacokinetic dosing-optimization study of current HIV antiretroviral regimens.
 900 *Antiviral Res*. 2018;159:45-54.
 901 87. Donner B, Niranjana V, and Hoffmann G. Safety of oseltamivir in pregnancy: a review of
 902 preclinical and clinical data. *Drug Saf*. 2010;33(8):631-42.
 903 88. Watanabe S, Tan NWW, Chan KWK, and Vasudevan SG. Assessing the utility of antivirals
 904 for preventing maternal-fetal transmission of zika virus in pregnant mice. *Antiviral Res*.
 905 2019;167:104-9.
 906 89. Sebghati M, and Khalil A. Uptake of vaccination in pregnancy. *Best Pract Res Clin Obstet*
 907 *Gynaecol*. 2021;76:53-65.
 908 90. Firouzbakht M, Sharif Nia H, Kazeminavaei F, and Rashidian P. Hesitancy about COVID-
 909 19 vaccination among pregnant women: a cross-sectional study based on the health
 910 belief model. *BMC Pregnancy Childbirth*. 2022;22(1):611.
 911 91. Kourtis AP, Read JS, and Jamieson DJ. Pregnancy and infection. *N Engl J Med*.
 912 2014;370(23):2211-8.
 913 92. Neu N, Duchon J, and Zachariah P. TORCH infections. *Clin Perinatol*. 2015;42(1):77-103,
 914 viii.
 915

916 **Figure Legends**

917 **Figure 1. maSCV2 infection of pregnant dams results in gestation-dependent morbidity.**

918 Nonpregnant adult females (A) or dams at embryonic day (E) 6 (B), E10 (C), and E16 (D) were
 919 intranasally inoculated with 10^5 TCID₅₀ of a mouse adapted SARS-CoV-2 (maSCV2) or mock
 920 inoculated with media. Following infection, mice were monitored for change in body mass and
 921 clinical signs of disease over fourteen days (A-D). Area under the curve (AUC) of body mass
 922 change curves for infected and uninfected animals were calculated, and then the AUC of
 923 infected animals was subtracted from the average AUC of mock animals of the same
 924 reproductive status and gestational age (E). Clinical scores given to animals included dyspnea,
 925 piloerection, hunched posture, and absence of an escape response and are quantified on a
 926 score of 0-4. The cumulative clinical score over the 14-day monitoring period is reported for
 927 each animal (F). Individual shapes (A-D) or bars (E-F) represent the mean (A-E) or median (F) ±

928 standard error of the mean (A-E) from two independent replications (n =7-13/group) with
 929 individual mice indicated by shapes (E-F). Significant differences ($p < 0.05$) were determined by
 930 two-way repeated measures ANOVA with Bonferroni post hoc test (A-F, to compare individual
 931 timepoints), two tailed unpaired t-test of AUCs (A-F, to compare across all timepoints), one-way
 932 ANOVA with Bonferroni post hoc test (E), or Kruskal-Wallis test (F) and are indicated by an
 933 asterisk (*).

934 **Figure 2. Pregnant dams infected during the third trimester-equivalent have reduced IFN-**
 935 **β responses, increased viral load, and reduced pulmonary function after infection.**

936 Nonpregnant adult females or dams at embryonic day (E) 6, E10, and E16 were intranasally
 937 inoculated with 10^5 TCID₅₀ maSCV2 or mock inoculated with media and euthanized at three
 938 days post infection (DPI) to collect maternal and fetal tissues. IFN β and viral titers in the right
 939 cranial lungs were measured using ELISA (A) and TCID₅₀ assay (B), respectively. Sections of
 940 fixed left lungs were stained by hematoxylin & eosin (H&E) to evaluate lung inflammation and
 941 images were taken at 20x magnification, with representative images of lungs maSCV2 or mock-
 942 inoculated at E16 shown (C). Asterisks (*) indicate intra-alveolar necrosis and inflammatory
 943 infiltrates, and arrows indicate peribronchiolar inflammatory infiltrates. Histopathological scoring
 944 was performed by a blinded board-certified veterinary pathologist to measure cumulative
 945 inflammation scores (D). A subset of mice were tracheostomized at three DPI to measure
 946 pulmonary function through the diffusion capacity for carbon monoxide (DF_{CO}) prior to
 947 euthanasia (E). Bars represent the mean (A-E) \pm standard error of the mean from at least two
 948 independent replications (n =4-11/group) with individual mice indicated by shapes. Significant
 949 differences ($p < 0.05$) were determined by two-way ANOVA with Bonferroni post hoc test
 950 (A,D,E) or one-way ANOVA with Bonferroni post hoc test (B) and are indicated by an asterisk
 951 (*). Scale bar: 100 μ m. LOD indicates the limit of detection.

952 **Figure 3. Third trimester-equivalent maSCV2 infection disrupts the trophoblast layer of**
 953 **the placental labyrinth zone and cytokine concentrations**

954 At embryonic day (E) 16, pregnant dams were intranasally inoculated with 10^5 TCID₅₀ of
 955 maSCV2 or mock inoculated with media and euthanized at 3 dpi to collect placentas.
 956 Representative H&E images (A) were taken at 5x (upper panels) and 20x magnification (lower
 957 panels, and specific areas of interest further zoomed 1.75 fold (black box). Within H&E-stained
 958 placentas, arrows indicate trophoblast giant cells and Ms indicate maternal blood spaces.
 959 Mononucleated trophoblast giant cells were identified and counted at 20x magnification (B).
 960 Placentas were immunostained for cytokeratin (C, red) to mark trophoblasts or vimentin (D, red)
 961 to mark endothelial cells and DAPI (blue) to label nuclei, with controls without primary antibody
 962 run in parallel. Representative images were taken at 20x magnification. Quantification of the
 963 percentage positive area for each marker is shown (E-F). Placentas were homogenized and
 964 analyzed by ELISA for IFN- β (G) IL-1 β (H). Bars represent the mean \pm standard error of the
 965 mean (n =5-10/group) with each shape indicating 1 placenta and, for analysis of images is the
 966 mean quantification or count of 6 fields of view. Significant differences ($p < 0.05$) were
 967 determined by unpaired two tailed t-test and are indicated by an asterisk (*). Scale bar: 1mm (A,
 968 upper panels/group), 40 μ m (A, lower panels/group), or 100 μ m (C-D)

969 **Figure 4. Third trimester-equivalent maSCV2 infection causes intrauterine growth**
 970 **restriction.**

971 At embryonic day (E) 6, E10, or E16, pregnant dams were intranasally inoculated with 10^5
 972 TCID₅₀ of maSCV2 or mock inoculated with media. At 3 dpi, a subset of dams were euthanized,
 973 and fetal viability was determined as the percentage of fetuses within the uterus (A, n= total
 974 number of fetuses from 8-12 dams per group from two independent replicates). Fetuses were
 975 counted as nonviable if they were smaller or discolored compared to gestational age-matched
 976 live fetuses or if a fetus was absent at an implantation site. A subset of dams were followed into
 977 the postnatal period to characterize adverse birth outcomes. At postnatal day 0 (PND0) overall
 978 litter size (B), pup mass (C), pup body length (D), and pup head diameter (E) were measured.
 979 Average measurements of each independent litter were graphed to account for litter effects (B-

980 E). Bars represent the mean \pm standard error of the mean from two independent replicates (n
 981 =7-14/group) with the average of individual litters indicated by shapes. Significant differences (p
 982 < 0.05) were determined by χ^2 (A) or two-way ANOVA with Bonferroni post hoc test (B-E) and
 983 are indicated by an asterisk (*).

984 **Figure 5. Offspring of dams infected with maSCV2 during the third trimester-equivalent**
 985 **display cortical thinning and reduced neurodevelopmental function.**

986 At embryonic day (E) 16, pregnant dams were intranasally inoculated with 10^5 TCID₅₀ of
 987 maSCV2 or mock inoculated with media. At PND0, a randomly selected subset of pups were
 988 euthanized via decapitation to collect fetal heads, which were fixed, sliced, and Nissl stained.
 989 Cortical thickness (A, red arrows) was measured from both brain hemispheres per pup and
 990 quantified as the average of 10 measurements per pup, with a single pup randomly chosen per
 991 dam (B, n=9-10 independent litters/group from 2 independent replicates). A subset of offspring
 992 were followed to PND5, sexed, and the neurobehavioral assays of surface righting (C), cliff
 993 aversion (D), and negative geotaxis (E) were performed to measure neurological development.
 994 1-2 pups per sex per dam were subjected to each test subsequently, with 3 trials given per test,
 995 and each pup's best trial for each test was reported (C-E, n=9-10 independent litters/group from
 996 2 independent replicates). Bars represent the mean \pm standard error of the mean with each
 997 shape indicating 1 pup. Significant differences ($p < 0.05$) were determined by unpaired two
 998 tailed t-test (B) or two-way ANOVA with Bonferroni post hoc test (C-E) and are indicated by an
 999 asterisk (*). Graphics built with Biorender.com.

1000 **Figure 6. Ritonavir-boosted nirmatrelvir mitigates maternal morbidity and reduced viral**
 1001 **titers in the lungs of pregnant dams.**

1002 Uninfected adult nonpregnant and pregnant (i.e., embryonic day (E)16) females were
 1003 euthanized, liver tissue collected, and western blots performed to quantify the amount of overall
 1004 CYP3A expression (A, n=4-5/group). At E16, pregnant dams or age-matched nonpregnant
 1005 females were intranasally infected with 10^5 TCID₅₀ of maSCV2 or mock inoculated with media.

1006 Starting at 4 hours post infection and continuing twice daily for 5 days or until tissue collection,
 1007 mice were treated with 1.7 mg nirmatrelvir and 0.6 mg ritonavir per dose or vehicle and were
 1008 monitored for changes in body mass for fourteen days (B, n=6/group from two independent
 1009 replicates). A subset of dams were euthanized at 3 dpi, and nasal turbinate and lung tissue
 1010 were collected, and viral titers were measured by TCID₅₀ assay (C-D, n=5-11/group). RNA was
 1011 extracted from lung homogenate, reverse transcribed using ProtoScript® II First Strand cDNA
 1012 Synthesis Kit, the M^{pro} region amplified, and Oxford Nanopore sequenced by Plasmidaurus.
 1013 Consensus sequences were imported and aligned to M^{pro} using ClustalO v1.2.3 in Geneious
 1014 Prime v2023.0.4. Alignments were imported into R v4.1.1., visualized, and annotated using
 1015 seqvisR v0.2.5 (E, n=4/group). Bars represent the mean ± standard error of the mean from two
 1016 independent replications with individual mice indicated by shapes (A,C,D). Significant
 1017 differences ($p < 0.05$) were determined by two tailed unpaired t-test (A), two-way ANOVA with
 1018 Bonferroni post hoc test of AUCs (B), or two-way ANOVA with Bonferroni post hoc test (C-D)
 1019 and are indicated by an asterisk (*). Sequence graphic built using Biorender.com. LOD indicates
 1020 the limit of detection.

1021 **Figure 7. Ritonavir-boosted nirmatrelvir prevents adverse offspring birth outcomes and**
 1022 **neurodevelopmental deficits associated with maternal maSCV2 infection.**

1023 At embryonic day (E)16, pregnant dams were intranasally inoculated with 10⁵ TCID₅₀ of
 1024 maSCV2 or mock inoculated with media. Starting at 4 hours post infection and continuing twice
 1025 daily for 5 days or until tissue collection, mice were treated with 1.7 mg nirmatrelvir and 0.6 mg
 1026 ritonavir per dose or vehicle. At PND0, a subset of pups were measured for pup mass (A), pup
 1027 length (B), and pup head diameter (C). Average measurements of each litter were graphed to
 1028 account for litter effects (A-C, n=6 independent litters/group from 2 independent replicates). A
 1029 subset of offspring were followed to PND5, sexed, and the neurobehavioral assays of surface
 1030 righting (D), cliff aversion (E), and negative geotaxis (F) were performed to measure
 1031 neurological development. 1-2 pups per sex per dam were subjected to each test subsequently,

1032 with 3 trials given per test, and each pup's best trial for each test was reported (D-F, n=6-8
1033 independent litters/group from 2 independent replicates). Bars represent the mean \pm standard
1034 error of the mean with each shape indicating litter's average (A-C) or pup (D-F). Significant
1035 differences ($p < 0.05$) were determined by two-way ANOVA with Bonferroni post hoc test (A-C)
1036 or three-way ANOVA with Bonferroni post hoc test (D-F) and are indicated by an asterisk (*).

bioRxiv preprint doi: <https://doi.org/10.1101/2023.03.28.533961>; this version posted June 25, 2023. The copyright holder for this preprint (which was not certified by peer review) is the author/funder. All rights reserved. No reuse allowed without permission.

Figure 1.

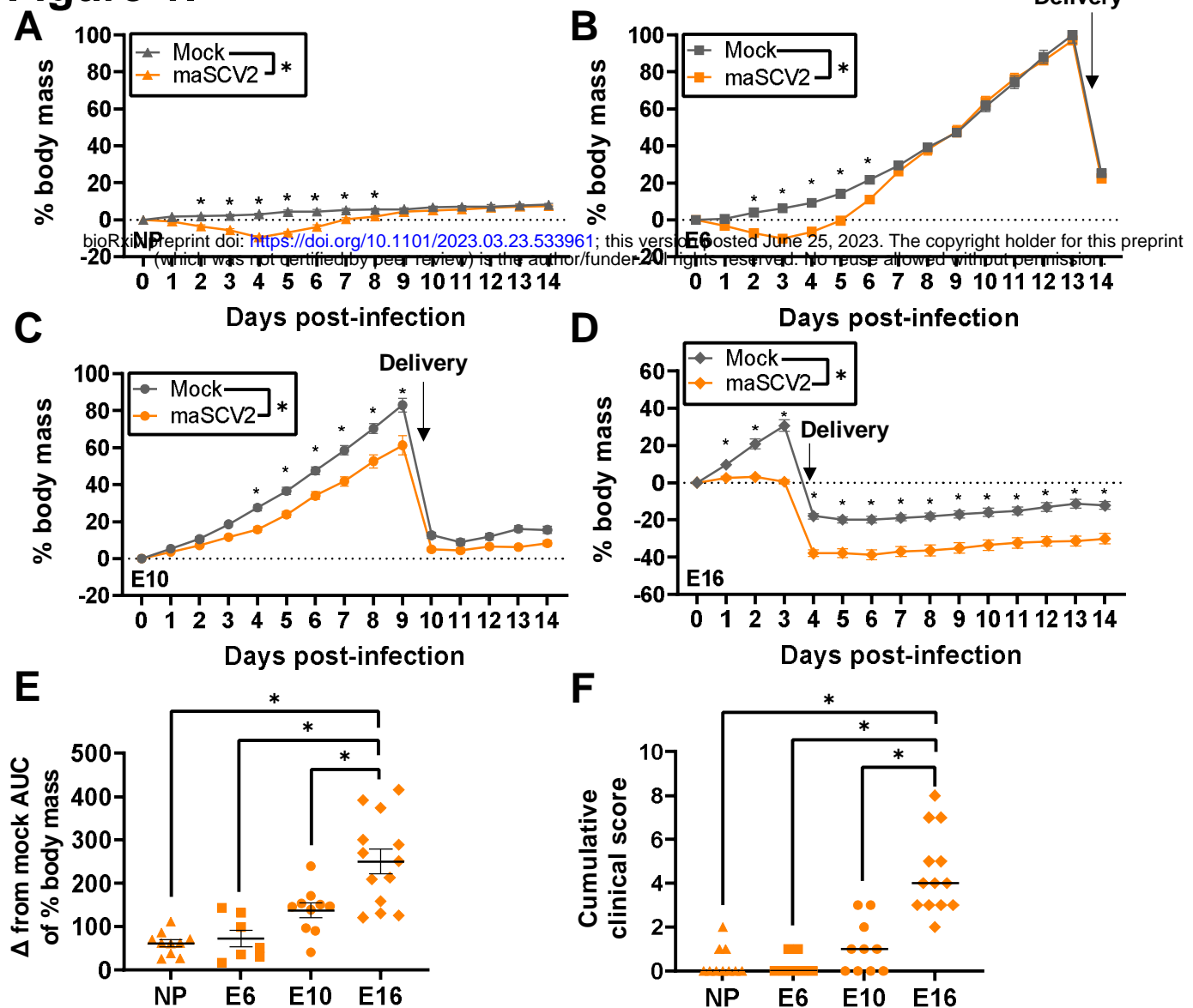


Figure 1. maSCV2 infection of pregnant dams results in gestation-dependent morbidity.

Nonpregnant adult females (A) or dams at embryonic day (E) 6 (B), E10 (C), and E16 (D) were intranasally inoculated with 10^5 TCID₅₀ of a mouse adapted SARS-CoV-2 (maSCV2) or mock inoculated with media. Following infection, mice were monitored for change in body mass and clinical signs of disease over fourteen days (A-D). Area under the curve (AUC) of body mass change curves for infected and uninfected animals were calculated, and then the AUC of infected animals was subtracted from the average AUC of mock animals of the same reproductive status and gestational age (E). Clinical scores given to animals included dyspnea, piloerection, hunched posture, and absence of an escape response and are quantified on a score of 0-4. The cumulative clinical score over the 14-day monitoring period is reported for each animal (F). Individual shapes (A-D) or bars (E-F) represent the mean (A-E) or median (F) \pm standard error of the mean (A-E) from two independent replications ($n = 7-13$ /group) with individual mice indicated by shapes (E-F). Significant differences ($p < 0.05$) were determined by two-way repeated measures ANOVA with Bonferroni post hoc test (A-F, to compare individual timepoints), two tailed unpaired t-test of AUCs (A-F, to compare across all timepoints), one-way ANOVA with Bonferroni post hoc test (E), or Kruskal-Wallis test (F) and are indicated by an asterisk (*).

Figure 2.

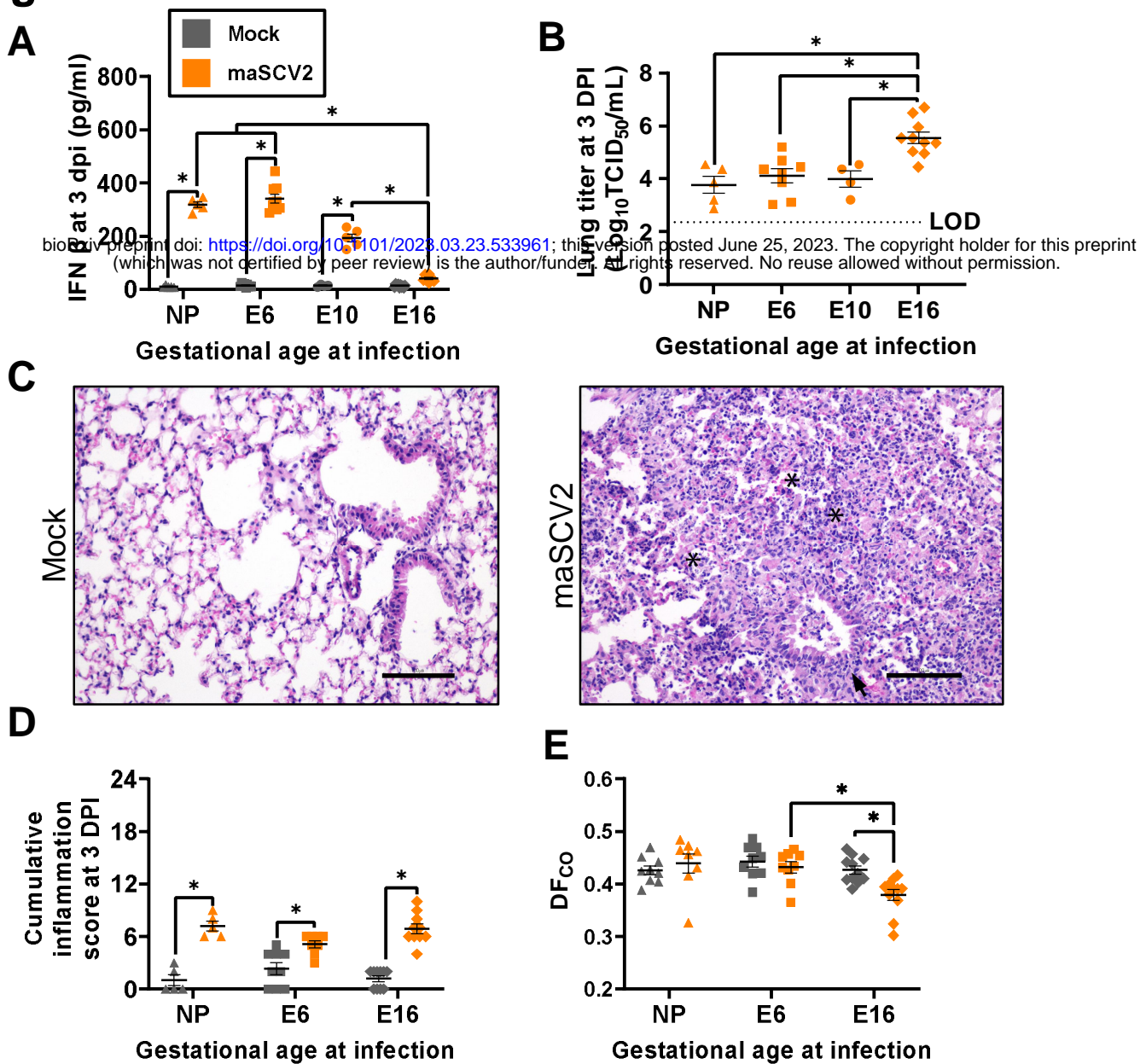


Figure 2. Pregnant dams infected during the third trimester-equivalent have reduced IFN- β responses, increased viral load, and reduced pulmonary function after infection.

Nonpregnant adult females or dams at embryonic day (E) 6, E10, and E16 were intranasally inoculated with 10^5 TCID₅₀ maSCV2 or mock inoculated with media and euthanized at three days post infection (DPI) to collect maternal and fetal tissues. IFN β and viral titers in the right cranial lungs were measured using ELISA (A) and TCID₅₀ assay (B), respectively. Sections of fixed left lungs were stained by hematoxylin & eosin (H&E) to evaluate lung inflammation and images were taken at 20x magnification, with representative images of lungs maSCV2 or mock-inoculated at E16 shown (C). Asterisks (*) indicate intra-alveolar necrosis and inflammatory infiltrates, and arrows indicate peribronchiolar inflammatory infiltrates. Histopathological scoring was performed by a blinded board-certified veterinary pathologist to measure cumulative inflammation scores (D). A subset of mice were tracheostomized at three DPI to measure pulmonary function through the diffusion capacity for carbon monoxide (DF_{CO}) prior to euthanasia (E). Bars represent the mean (A-E) \pm standard error of the mean from at least two independent replications (n =4-11/group) with individual mice indicated by shapes. Significant differences ($p < 0.05$) were determined by two-way ANOVA with Bonferroni post hoc test (A,D,E) or one-way ANOVA with Bonferroni post hoc test (B) and are indicated by an asterisk (*). Scale bar: 100 μ m. LOD indicates the limit of detection.

Figure 3.

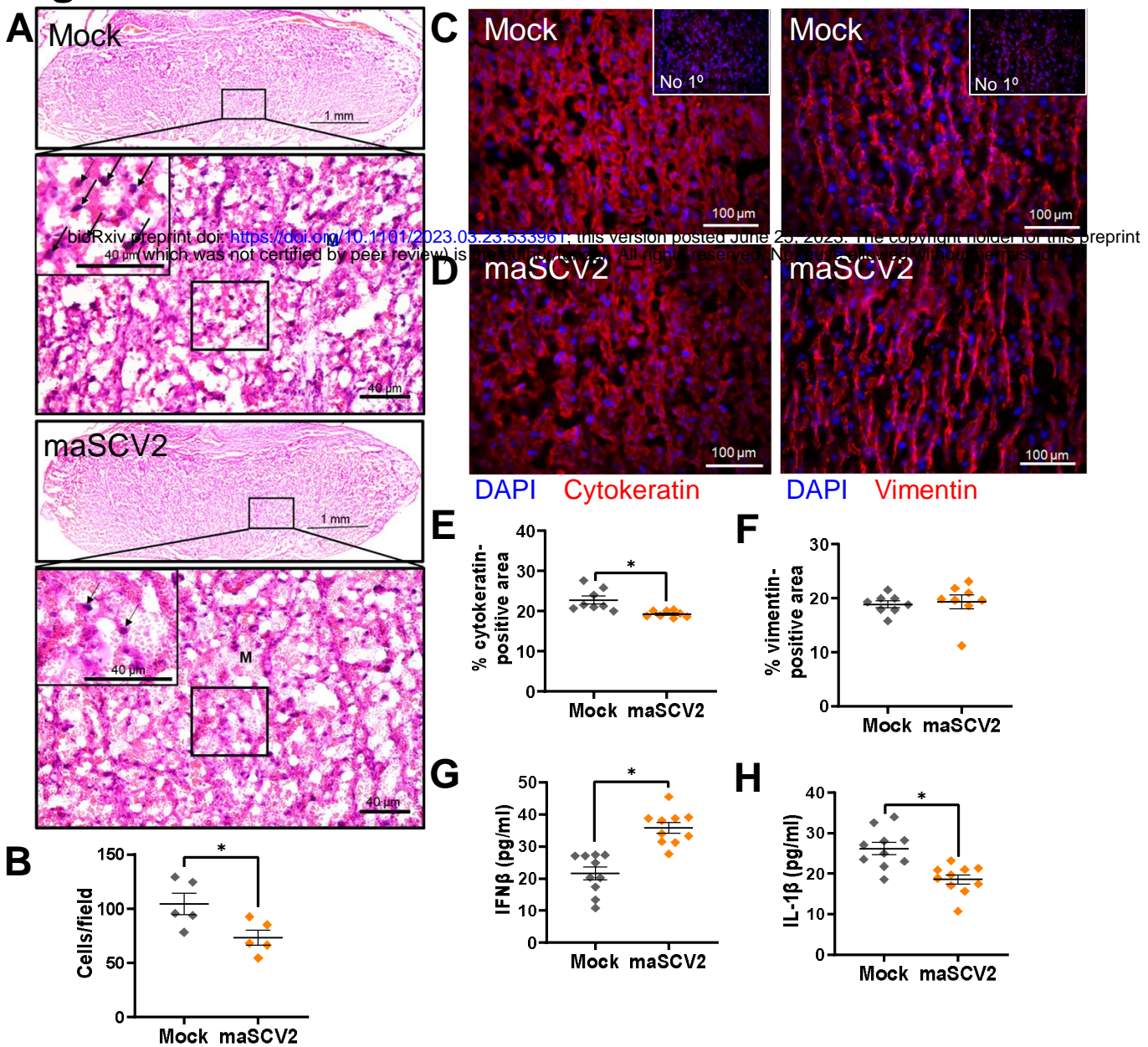


Figure 3. Third trimester-equivalent maSCV2 infection disrupts the trophoblast layer of the placental labyrinth zone and cytokine concentrations

At embryonic day (E) 16, pregnant dams were intranasally inoculated with 10^5 TCID₅₀ of maSCV2 or mock inoculated with media and euthanized at 3 dpi to collect placentas. Representative H&E images (A) were taken at 5x (upper panels) and 20x magnification (lower panels, and specific areas of interest further zoomed 1.75 fold (black box)). Within H&E-stained placentas, arrows indicate trophoblast giant cells and Ms indicate maternal blood spaces. Mononucleated trophoblast giant cells were identified and counted at 20x magnification (B). Placentas were immunostained for cytokeratin (C, red) to mark trophoblasts or vimentin (D, red) to mark endothelial cells and DAPI (blue) to label nuclei, with controls without primary antibody run in parallel. Representative images were taken at 20x magnification. Quantification of the percentage positive area for each marker is shown (E-F). Placentas were homogenized and analyzed by ELISA for IFN- β (G) IL-1 β (H). Bars represent the mean \pm standard error of the mean ($n = 5-10$ /group) with each shape indicating 1 placenta and, for analysis of images is the mean quantification or count of 6 fields of view. Significant differences ($p < 0.05$) were determined by unpaired two tailed t-test and are indicated by an asterisk (*). Scale bar: 1 mm (A, upper panels/group), 40 μ m (A, lower panels/group), or 100 μ m (C-D)

Figure 4.

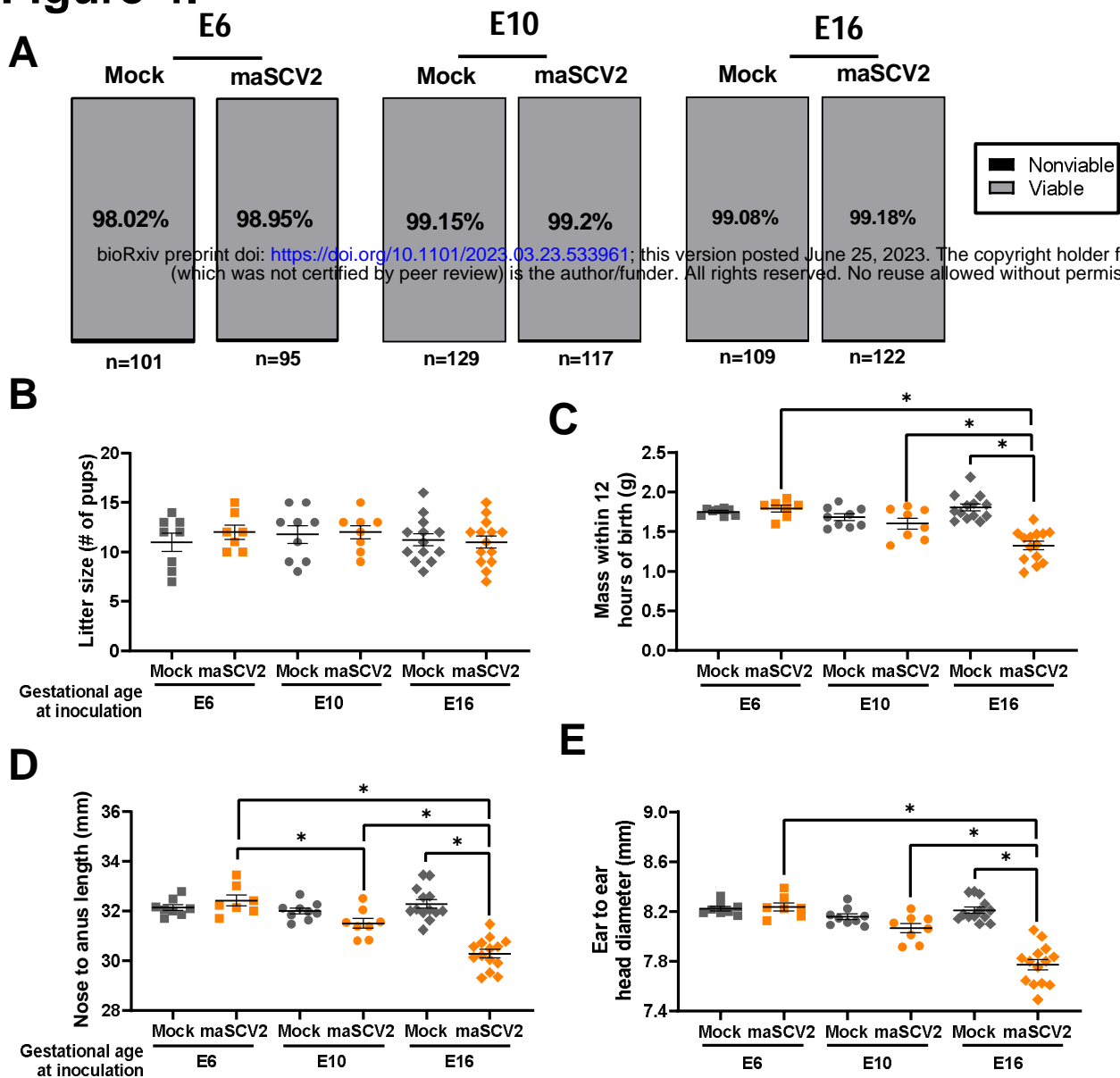


Figure 4. Third trimester-equivalent maSCV2 infection causes intrauterine growth restriction.

At embryonic day (E) 6, E10, or E16, pregnant dams were intranasally inoculated with 10^5 TCID₅₀ of maSCV2 or mock inoculated with media. At 3 dpi, a subset of dams were euthanized, and fetal viability was determined as the percentage of fetuses within the uterus (A, n = total number of fetuses from 8-12 dams per group from two independent replicates). Fetuses were counted as nonviable if they were smaller or discolored compared to gestational age-matched live fetuses or if a fetus was absent at an implantation site. A subset of dams were followed into the postnatal period to characterize adverse birth outcomes. At postnatal day 0 (PND0) overall litter size (B), pup mass (C), pup body length (D), and pup head diameter (E) were measured. Average measurements of each independent litter were graphed to account for litter effects (B-E). Bars represent the mean \pm standard error of the mean from two independent replicates (n = 7-14/group) with the average of individual litters indicated by shapes. Significant differences ($p < 0.05$) were determined by χ^2 (A) or two-way ANOVA with Bonferroni post hoc test (B-E) and are indicated by an asterisk (*).

Figure 5.

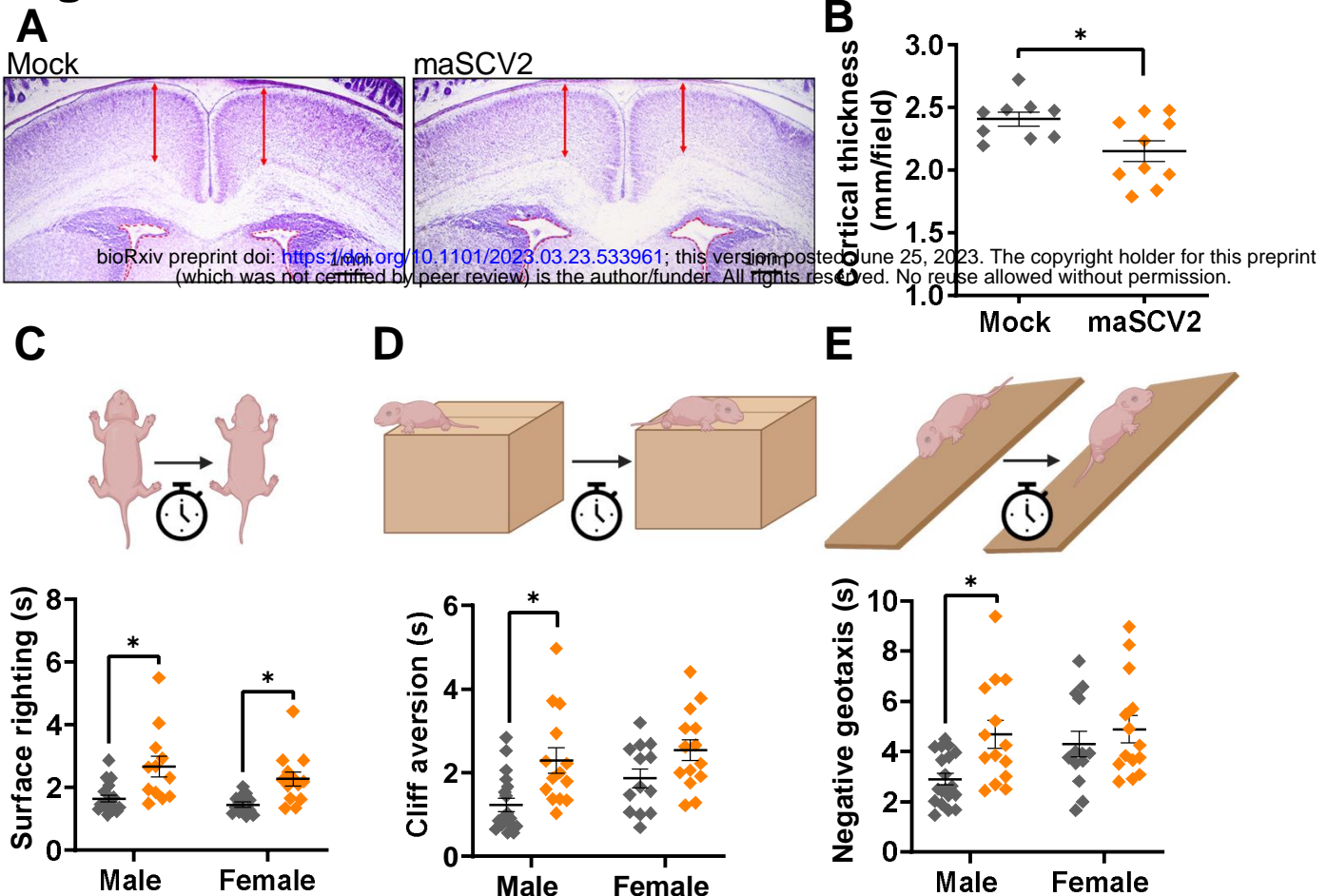
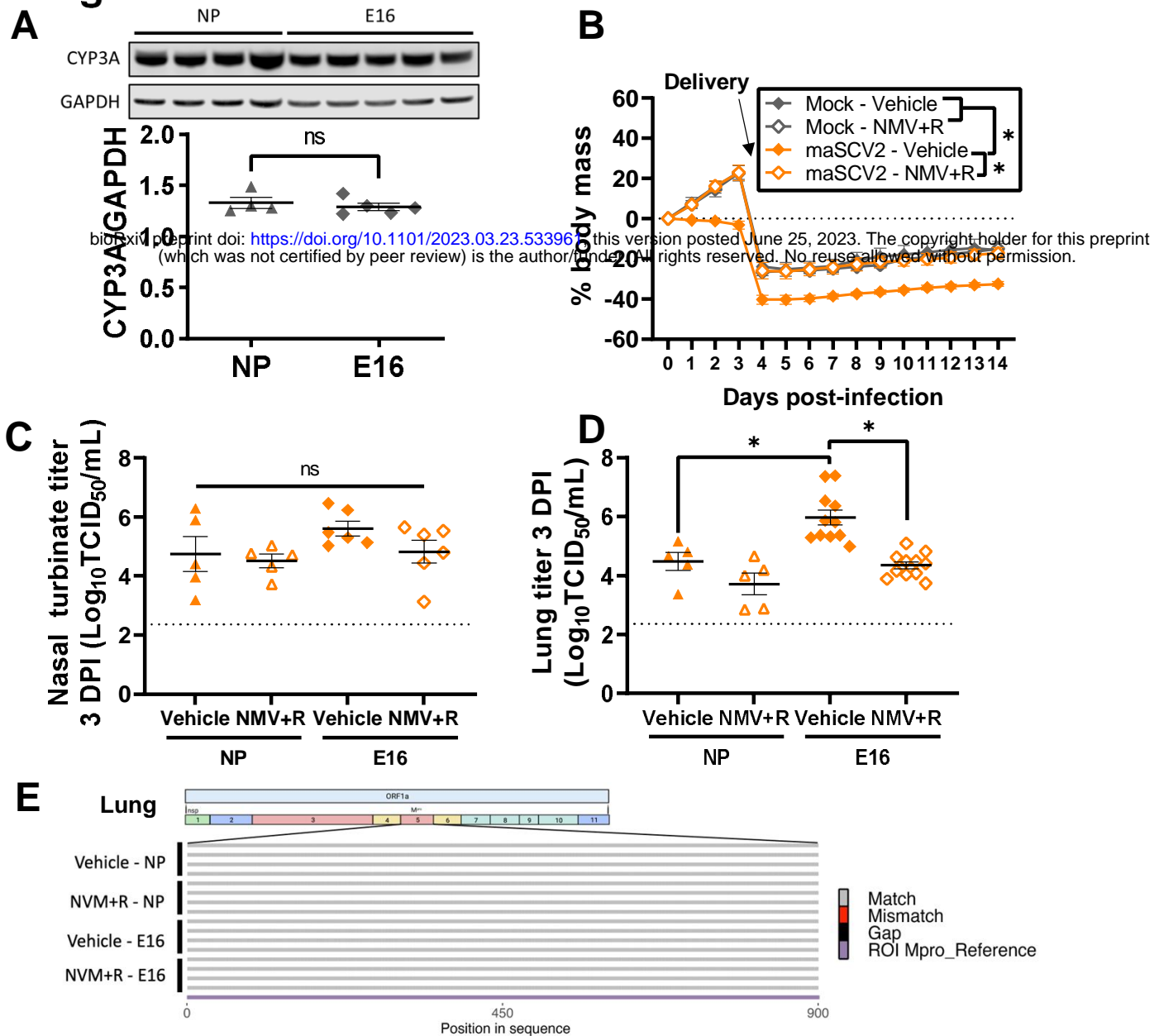


Figure 5. Offspring of dams infected with maSCV2 during the third trimester-equivalent display cortical thinning and reduced neurodevelopmental function.

At embryonic day (E) 16, pregnant dams were intranasally inoculated with 10^5 TCID₅₀ of maSCV2 or mock inoculated with media. At PND0, a randomly selected subset of pups were euthanized via decapitation to collect fetal heads, which were fixed, sliced, and Nissl stained. Cortical thickness (A, red arrows) was measured from both brain hemispheres per pup and quantified as the average of 10 measurements per pup, with a single pup randomly chosen per dam (B, n=9-10 independent litters/group from 2 independent replicates). A subset of offspring were followed to PND5, sexed, and the neurobehavioral assays of surface righting (C), cliff aversion (D), and negative geotaxis (E) were performed to measure neurological development. 1-2 pups per sex per dam were subjected to each test subsequently, with 3 trials given per test, and each pup's best trial for each test was reported (C-E, n=9-10 independent litters/group from 2 independent replicates). Bars represent the mean \pm standard error of the mean with each shape indicating 1 pup. Significant differences ($p < 0.05$) were determined by unpaired two tailed t-test (B) or two-way ANOVA with Bonferroni post hoc test (C-E) and are indicated by an asterisk (*). Graphics built with Biorender.com.

Figure 6.**Figure 6. Ritonavir-boosted nirmatrelvir mitigates maternal morbidity and reduced viral titers in the lungs of pregnant dams.**

Uninfected adult nonpregnant and pregnant (i.e., embryonic day (E)16) females were euthanized, liver tissue collected, and western blots performed to quantify the amount of overall CYP3A expression (A, n=4-5/group). At E16, pregnant dams or age-matched nonpregnant females were intranasally infected with 10^5 TCID₅₀ of maSCV2 or mock inoculated with media. Starting at 4 hours post infection and continuing twice daily for 5 days or until tissue collection, mice were treated with 1.7 mg nirmatrelvir and 0.6 mg ritonavir per dose or vehicle and were monitored for changes in body mass for fourteen days (B, n=6/group from two independent replicates). A subset of dams were euthanized at 3 dpi, and nasal turbinate and lung tissue were collected, and viral titers were measured by TCID₅₀ assay (C-D, n=5-11/group). RNA was extracted from lung homogenate, reverse transcribed using ProtoScript[®] II First Strand cDNA Synthesis Kit, the M^{PRO} region amplified, and Oxford Nanopore sequenced by Plasmidaurus. Consensus sequences were imported and aligned to M^{PRO} using ClustalO v1.2.3 in Geneious Prime v2023.0.4. Alignments were imported into R v4.1.1., visualized, and annotated using seqvisR v0.2.5 (E, n=4/group). Bars represent the mean \pm standard error of the mean from two independent replications with individual mice indicated by shapes (A,C,D). Significant differences ($p < 0.05$) were determined by two tailed unpaired t-test (A), two-way ANOVA with Bonferroni post hoc test of AUCs (B), or two-way ANOVA with Bonferroni post hoc test (C-D) and are indicated by an asterisk (*). Sequence graphic built using Biorender.com. LOD indicates the limit of detection.

Figure 7.

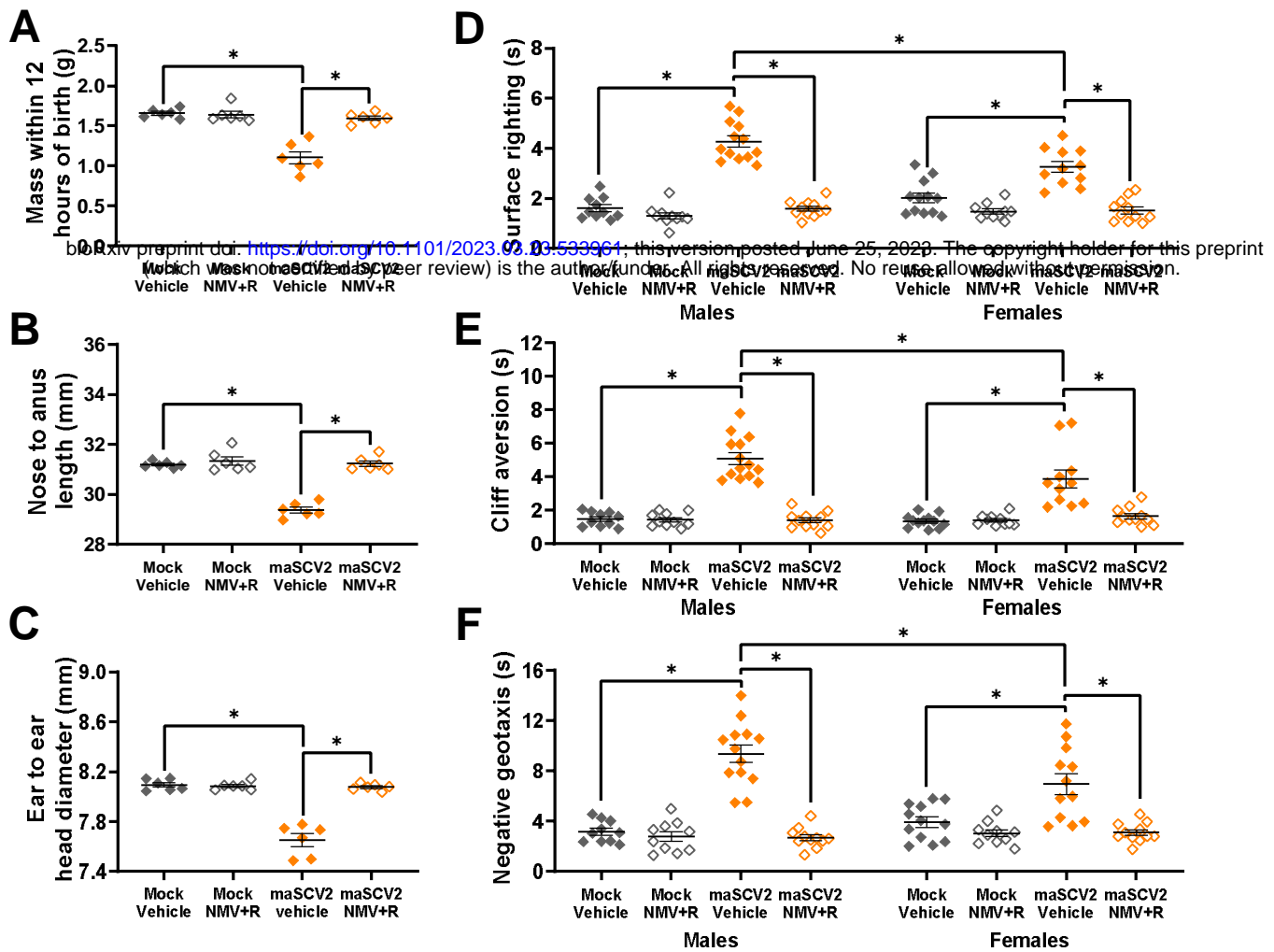


Figure 7. Ritonavir-boosted nirmatrelvir prevents adverse offspring birth outcomes and neurodevelopmental deficits associated with maternal maSCV2 infection.

At embryonic day (E)16, pregnant dams were intranasally inoculated with 10^5 TCID₅₀ of maSCV2 or mock inoculated with media. Starting at 4 hours post infection and continuing twice daily for 5 days or until tissue collection, mice were treated with 1.7 mg nirmatrelvir and 0.6 mg ritonavir per dose or vehicle. At PND0, a subset of pups were measured for pup mass (A), pup length (B), and pup head diameter (C). Average measurements of each litter were graphed to account for litter effects (A-C, n=6 independent litters/group from 2 independent replicates). A subset of offspring were followed to PND5, sexed, and the neurobehavioral assays of surface righting (D), cliff aversion (E), and negative geotaxis (F) were performed to measure neurological development. 1-2 pups per sex per dam were subjected to each test subsequently, with 3 trials given per test, and each pup's best trial for each test was reported (D-F, n=6-8 independent litters/group from 2 independent replicates). Bars represent the mean \pm standard error of the mean with each shape indicating 1 litter's average (A-C) or 1 pup (D-E). Significant differences ($p < 0.05$) were determined by two-way ANOVA with Bonferroni post hoc test (A-C) or three-way ANOVA with Bonferroni post hoc test (D-F) and are indicated by an asterisk (*).